In-process Monitoring and Qualification of SLM Produced Nickel Based Superalloys Using Eddy Current Inspection Method and a Novel EC Array Probe Design

by

Erdem Bektaş

A Dissertation Submitted to the Graduate School of Sciences and Engineering in Partial Fulfillment of the Requirements for the Degree of Doctor of Philosophy

in

Mechanical Engineering

KOÇ ÜNİVERSİTESİ

August 5, 2022

In-process Monitoring and Qualification of SLM Produced Nickel Based Superalloys Using Eddy Current Inspection Method and a Novel EC Array Probe Design

Koç University

Graduate School of Sciences and Engineering

This is to certify that I have examined this copy of a doctoral dissertation by

Erdem Bektaş

and have found that it is complete and satisfactory in all respects,

and that any and all revisions required by the final

examining committee have been made.

Committee Members:

____

Prof. Dr. Demircan Canadinç (Advisor)

____

Prof. Dr. İsmail Lazoğlu

____

Assoc. Prof. Dr. Uğur Ünal

____

Assoc. Prof. Dr. Burak Bal

____

Assist. Prof. Dr. Sıdıka Mine Toker

Date: ______________________________________

ABSTRACT

In-process Monitoring and Qualification of SLM Produced Nickel Based Superalloys Using Eddy Current Inspection Method and a Novel EC Array Probe Design

Erdem Bektaş

Doctor of Philosophy in Mechanical Engineering

August 5, 2022

Additive manufacturing gives high flexibility to part designers on the manufacturability of optimized and complex parts. This advantage brings a part inspectability challenge. In this study, the Eddy Current Array sensor application is investigated as an in-process monitoring/inspection method and discussed as an L-PBF layer acceptance technique for the volumetric qualification of aerospace parts. Laser Powder Bed Fusion (L-PBF) process produced Inconel 625 test samples are used for data collection. Intentionally defects are created by using a waterjet-guided laser system to trial the L-PBF in-process eddy current inspection capability.

ÖZETÇE

SLM Metodu ile Üretilmiş Nikel Bazlı Süperalaşımların Girdap Akımı Metodu ile Proses İçi Takibi ve Kalifiye Edilmesi ve Yeni Bir EC Seri Prob Tasarımı

Erdem Bektaş

Makine Mühendisliği, Doktora

5 Ağustos 2022

Eklemeli imalat teknolojisi, tasarımcılara optimize edilmiş ve karmaşık parçaların üretilebilirliği açısından yüksek esneklik avantajı kazandırmaktadır. Bu avantaj aynı zamanda muayene edilebilirlik zorluğunu da getirmektedir. Bu çalışmada Girdap Akımı Sıra Sensör uygulaması, proses içi gözlem/muayene metodu olarak incelenmiş ve L-PBF katman kabul tekniği olarak kullanılması ve bu uygulamada üretilen havacılık-uzay parçalarının hacimsel bir kalifiye etme aracı olarak kullanılması tartışılmıştır. Toz yatağında lazer birleştirme (ing. Laser Powder Bed Fusion – L-PBF) prosesi ile üretilmiş Inconel 625 test parçaları data toplanması için kullanılmıştır. L-PBF proses içi girdap akımı muayene yönteminin kabiliyet testlerini değerlendirebilmek için test parçalarında su-jeti yönlendirmeli lazer sistemi ile kasti hatalar oluşturulmuştur.

ACKNOWLEDGMENTS

Firstly, I would like to heartfully thank my advisor Prof. Dr. Demircan Canadinç, for his deep patience, motivation, and continuous support for me. His technical and procedural knowledge always proceeded me one step further. Without his help, I would not be able to finish this thesis.

Besides my advisor, I would like to thank my thesis committee members, Prof. Dr. İsmail Lazoğlu and Assoc. Prof. Uğur Ünal for their valuable comments, questions, and support during this study.

Additionally, I would like to thank a lot of people from TEI (Tusas Engine Industries Inc.); Technology Programs Manager Güray Akbulut, and Additive Manufacturing Team Leader Akın Orhangül for supporting the production of test parts, Barış Pehlivanoğulları for manufacturing test parts on EOS M290 machine, Mehmet Yüksel for making the grinding, Levent Subaşı and Aydemir Günaydın for implementing defects to sample details on Synova Laser waterjet system, Soner Akın and Çağdaş Şen for measurements on ATOS 3D scanner and 3D point cloud generation, Ceren Şen for running AM production simulations for deflection predictions.

I want to express my gratitude to Eddyfi Technologies, especially to Zeki Coşku Gökçe for letting their Ectane 2 instrument for data collection and Matthew Wolf for the setup of the instrument, technical support, and advice.

My sincere thanks go to Uniwest and Kurt E. Oldson for donating the EC probe and cable for data collection.

I also thank Fatma Ünal, Ali Ünal, and Pınar Ünal for helping with the logistics of the test instruments, Tamer Türkücü, Barış Gençer, Kutsal Akdağ and Sude Akdağ for their valuable efforts on approval of this thesis.

Lastly, I would like to thank my parents, my brother, my wife, and my daughter for supporting me all my life and while writing this thesis.

TABLE OF CONTENTS

LIST OF TABLES

LIST OF FIGURES

ABBREVIATIONS

AM	Additive Manufacturing
CSV	Comma Separated Values
DED	Directed Energy Deposition
DoD	Department of Defense
DMLM	Direct Metal Laser Melting
H	Henry
Hz	Hertz
L-PBF	Laser Powder Bed Fusion
m	Meter
mm	Millimeter
NDT	Non-Destructive Testing
S	Siemens
SLM	Selective Laser Melting (a.k.a. L-PBF)
µm	Micrometer

Chapter 1

INTRODUCTION

1.1. Overview

Additive Manufacturing (AM) is one of the most trending manufacturing methods in 21st century. AM's usage has significantly increased from individual hobbyists to global corporate companies. AM has been mainly adopted by aerospace, transportation, medical, energy, and consumer products industries [1]. The additive manufacturing process offers a wide variety of materials such as tissues, concrete, plastics, composites, metals, and metal alloys. [2]

Metal alloys are highly used in structures requiring high strength. Conventional machining of metal alloys requires casting, forging, rolling, metal forming, and subtractive manufacturing methods such as turning and milling. All these processes have limits on shaping metal alloys, so designers must consider the constraints of these methods on the finished shape. Additive manufacturing for shaping metal alloys gives designers significant advantages in design possibilities. The limits of conventional machining techniques are not a boundary for designers anymore.

Design advantages [3], rapid production capability, high fly-to-buy ratio, and compatibility with weldable nickel superalloys make additive manufacturing also a trending process for aerospace part manufacturers. 3D printed parts on aerospace vehicles are increasing day to day.

One of the significant problems of additive manufactured parts is qualifying [4]. Critical aerospace parts must be inspected volumetrically, and critical surfaces should be checked to be assured that there is no defect greater than the design limits within the part. Application of conventional inspection methods is very difficult or impossible due to surface roughness and topological optimized complex shapes of AM parts.

When an AM manufactured part is post-process inspected and not accepted, or it is not post-process inspectable, this is a significant loss of time, powder, money, and motivation. In-process monitoring techniques are used to put process parameters on track and catch anomalies that may lead to defects. In the future, when an anomaly will be located, a local repair or further layer processes may also be applied to eliminate possible defects.

Can a process be applied to selective laser melting (SLS), also known as laser powder bed fusion (L-PBF) additive manufacturing devices to work as an in-process monitoring/inspection method and as a volumetric inspection method that will assure the part leaving the AM process? This is one of the demanded and unanswered questions on additive manufacturing and the motivation of this thesis.

1.2. Motivation

Additive manufacturing struggles with qualification and certification of parts. Especially critical aerospace parts, either conventionally or additively manufactured, need 100% volumetric and surface quality approval before being installed on an aero vehicle. The primary motivation of this study is to show an acceptable means of qualification for aerospace production parts before leaving the AM device. If an additive manufacturing device has an approved qualification apparatus, it will be a tremendous advantage for part producers.

There is still no common standard for inspecting, accepting or certifying additive manufactured aerospace parts. The studies and discussions are still ongoing. The commonly preferred post-process inspection method is Computed Tomography (CT) which is expensive, time demanding, and thick material inspection is not as sensitive as thin material inspection. Other than post-process inspection, there are some commercial sensor packages and software (generally sold with additive manufacturing machines) and process parameters' follow-up for process optimization and in-process monitoring.

Additive manufacturing has great potential for aerospace parts production, but it has a much brighter future at separated production sites such as spare parts for old vehicles or far-field production places; ships, islands, and even outer space orbital stations, moon, Mars, and beyond.

All these future manufacturing sites will probably strictly demand the usage of only a few machines for production because of a lack of resources, cost, maintainability, and efficiency. Hopefully, an additive manufacturing solution with in-process monitoring/inspection and volumetric part qualification capability will fulfill most of the quality demands for onsite and separated production places. An in-process monitoring method with a conventional non-destructive testing foundation looks promising based on its physical abilities.

One of the NDT methods, Eddy current inspection method, is a surface and near-surface (thin subsurface) inspection method, with inspection depths similar to a few powder bed layer thicknesses and laser re-solidification depths. Combining these, inspecting and qualifying every re-solidified layer of the L-PBF process will mean volumetric inspection and qualification of the whole part at the end of the process.

There are two main pushing motivations for the thesis. Firstly, the idea that eddy current inspection is the most suitable method for error-proofing the melted and re-solidified layer. Second, the motto "trust is good, but control is better" should be understood in powder bed additive manufacturing as; trusting the verified margins of process monitoring (in-process monitoring) is good but controlling every build layer by checking the material continuity is much better. The concept in this work can also be identified as in-process control and inspection rather than just an in-process monitoring method.

In addition to the reasons mentioned above, another motivation is the future assumed trend for the cost control of the L-PBF process. For example, consumer electronics manufacturing, especially the electronic display production industry, had difficulties with supply when screen sizes increased. The price of flat screens grew exponentially with the growing screen size. The leading cause for this was necessary pixel numbers were increasing, and if some pixels had to error, producers could not sell out screen. As the number of pixels increased, the possibility of getting a bad pixel chance increased. So, the cost of producing an excellent display increased much faster than the increase in the pixel number. The flat screen industry decreased the cost of production by finding and repairing the bad pixels during production [5]. The Additive manufacturing industry uses millions of powder grains to produce a part like millions of pixels on a flat screen. In state-of-the-art today, identifying defects and stopping the building may be the achievable target to control increasing costs. Sooner or later, the industry cost competition will demand more cost savings, and just stopping the build will not be enough. The process control will evolve to find defects and make an in-process repair; at this moment, an acceptable inspection of the part will be necessary. It should collect data directly from the part rather than the process parameters. The proposed method in this study can be an acceptable and appropriate address for this future need.

The study herein gives a solution for in-process monitoring (also control and inspection) and volumetric inspection of SLM-manufactured aerospace alloys. The proposed method will qualify the parts leaving the laser powder bed AM device.

1.3. Objective of The Study

The thesis objective is to develop a state-of-the-art in-process monitoring and inspection method that will assure the quality of the additively manufactured parts, leaving the laser powder bed AM machine in means of metallurgical integrity and mechanical strength.

The study herein is limited to concept proof of the application on Inconel 625 alloy, a nickel-based aerospace superalloy. However, the method can be used widespread along with other nickel-based or non-nickel-based aerospace alloys.

The thesis is concept proofing the usage of an eddy current array probe with a unique multi-coil positioning setup. The eddy current array probe will be responsible for collecting the data from the AM part surface and near sub-surface through non-destructive testing. Real-time image reconstruction of collected data will bring the magnetic response map of the surface. Image analysis will check the defect locations (pores, cracks, voids, unmelted regions, etc.).

In the future, if an intercommunication between SLM control and in-process monitoring/inspection system will be set and be able to handle the defects with repair possibilities (Figure 1.1) such as; re-melting, more/less energy input at next layer melting, or changing scan & laser input power strategies, or repair with additional modification miniature arms like laser cladding/milling.

The above mentioned in-process monitoring system will decrease the defects by in-process defect location proposals, increase productivity and qualify the part “on base plate” condition.

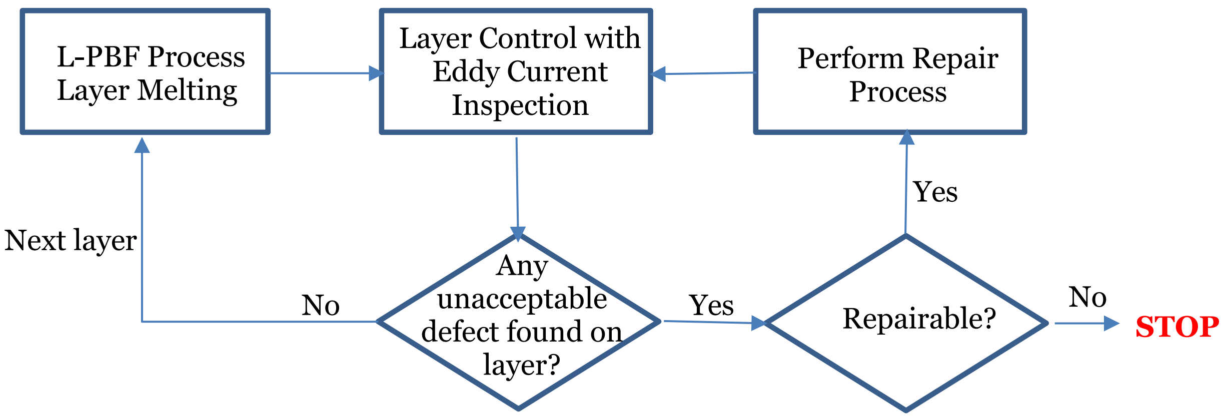

Figure 1.1 Place of Eddy Current inspection in the future L-PBF process

Chapter 2

CURRENT STATE OF THE ART

2.1 *Additive Manufacturing*

Additive manufacturing has a wide variety of usage in demanding industries such as healthcare, energy, aviation, aerospace, defense, construction, personal hobbyists, etc. All these industries require different types of engineering materials. Since plastics, composites, and living tissues are out of the scope of this study, high-performance material demanding applications such as aerospace requires metals in specific aerospace alloys.

Additive manufacturing of aerospace alloys depends on; Direct energy deposition and powder bed fusion (aka SLM) processes.

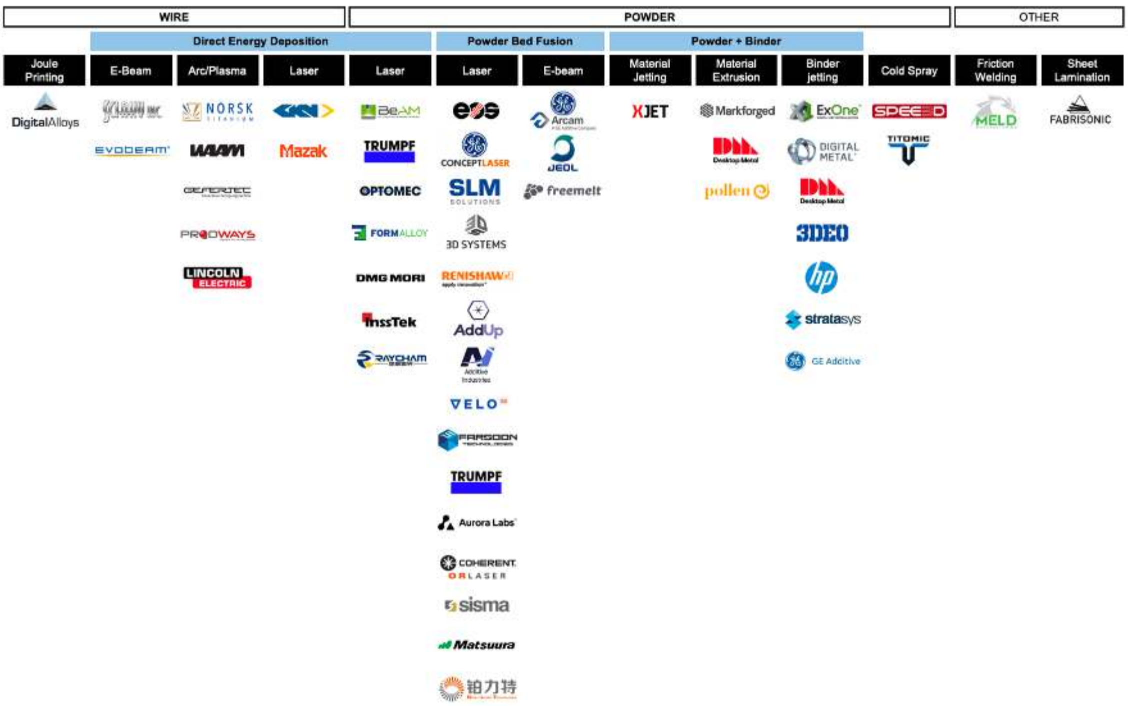

Figure 2.1 Metal additive manufacturing processes and companies [6]

Figure 2. shows Direct Energy Deposition (DED) energy sources can be E-Beam,

Arc/Plasma, or laser. Both the energy and metal must be directed and merged in their addition place. After a successful fusion, a new metal piece should have been welded to its new position. In powder bed fusion, an electron beam (E-Beam) or laser beam can be used as an energy source. Unlike DED, the powder is spread as a layer on top of the previous layer, and only the energy source moves along material melting points on the layer. The energy paths are welded, and unwelded powder can be filtered and reused in future processes.

2.2 Selective Laser Melting

Selective laser melting (SLM), also known as laser powder bed fusion (L-PBF), is an additive manufacturing method using metal powder and a laser energy source for powder melting. Fusion of melted powder under a highly controlled environment brings 3D printing of parts layer by layer with a high-speed micro welding process. Its acceptance and ownership are increasing day to day. Significant studies and developments are made to mature the technology, and there is more way to go for supply chain, simulation, manufacturing process, post processes, and certification.

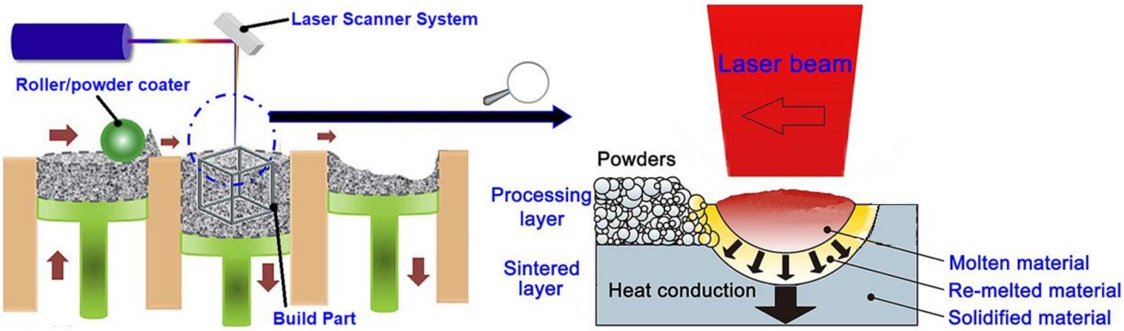

Figure 2.2 Selective laser melting schematic (after [7])

It is evident that SLM or 3D printing will have effects on the supply chain. SLM needs a reliable supply chain of powder material. But other than the process supply chain, SLM will significantly change the product supply chain. Arbabian and Wagner investigate the market changes based on some scenarios and if the manufacturer or retailer would adopt a 3D printing machine [8].

Stolt et al. describe the strong relationship between manufacturing and design for SLM. They suggest that the cost of 3D printing can change significantly based on design alternatives, and the options should be identified in the early stages of design. They also discuss that the designs that cannot be inspected after production must be reworked or stopped [9].

Although SLM is a very productive and flexible process, it has some disadvantages to conventional production methods, such as confidence in the process part.

King et al. point out the lack of confidence in the quality of the laser powder bed fusion additive manufactured parts. They claim that confidence can be established by understanding the fundamental physics of the process, mainly by modeling and simulation. They discuss their simulation results on powder scale and part scale sizes and point out the difficulties of successful predictive modeling. [7]

Residual stresses have an essential effect on the deflection of parts during additive manufacturing. Residual stresses may occur from different phenomena such as temperature differences and transient temperatures. Kundakcioglu et al. comment on the need for simulation tools for SLM, investigate the simulation capabilities for thermal modeling and transient temperatures during build up, and compare results with experimental Ti-6Al-4V and Inconel 625 alloys [10], [11].

Tepylo et al. investigate the laser-based additive manufacturing technologies for aerospace applications and point out that traditional Non-Destructive Inspection techniques may not work for AM parts, and new methods will be needed [12].

Although Computed Tomography (CT) is a currently used post-process Non-Destructive inspection method for L-PBF parts, its some disadvantages have been reported, such as numerous variables influence qualitative results, has no general standards, the appearance of non-real brightness causes loss of measurement capacity, and lack of traceability [13].

To increase the process control and decrease the part defects, various kinds of in-process monitoring methods are under use and development, commercially in use or still at labs.

2.3 Commercial In-Process Monitoring Methods

Commercially available in-process methods are the ones that are already installed in a commercial powder bed laser additive manufacturing system or a third-party solution that is available in the market that can be bought and installed in an additive manufacturing system separately. The first group is generally given as an option by system manufacturers. Some methods are Arcam’s XLayerQam, Concept Laser’s QM Coating and QM Meltpool 3D modules, EOS's EOSTATE Meltpool Monitoring and Exposure OT.

Arcam company has solutions in powder bed additive manufacturing both for laser and electron beam energy sources. They offer XLayerQam for the detection of porosity and defects at each layer. It uses a high-resolution camera for image collection.

Concept Laser's Quality Management (QM) Modules for inline process monitoring are QM Coating and QM Melt Pool 3D. QM Coating Module controls the dose factor of the powder automatically; in other means, it changes the thickness of each layer for the optimum build-up and to decrease process time. [14]

QM Melt Pool 3D module detects the emissions from the melt pool with the help of a coaxial sensor. The tool determines the size and intensity of the melt pool. This method can detect possible process flaws.

Like Concept Laser, EOS also uses a melt pool monitoring method named EOSTATE Melt Pool. It uses a photodiode to measure the light emitted from the melt pool. This method monitors process deviations based on location points [15].

EOS also offers Optical Tomography tool named EOSTATE Exposure OT. The method is a visual non-destructive testing method of each layer by image collection. The tool also measures the heat emission of built space in real-time. The tool helps users to decrease quality assurance costs by identifying possible defect locations before serial production [16].

In addition to the commercially available in-process monitoring methods mentioned above, there is ongoing research on in-process monitoring technologies and methods.

2.4 Recent Studies on In-Process Monitoring

Studies about in-process monitoring continue, and no commonly accepted method is available. The in-process monitoring has been identified as a technology gap subject that progress is still demanded. The in-situ monitoring technology gap also requires improvement of sub-items: in-situ process sensing/monitoring capabilities, closed-loop process control development, and advanced data collection & analysis [17].

The sensor technologies of in-process monitoring technologies under progress are optical imaging, thermal imaging, spectrometer, thermocouple, displacement sensors, ultrasonic, eddy current, accelerometer, microphone, electric circuit, X-Ray, and neutron diffraction [18]. Besides the variety of methods mentioned above, significant efforts are made on optical and thermal imaging methods in literature [19]–[24], and optical imaging is reported as having the most advanced technology readiness level along other methods [18].

Mohr et al. investigated the combination of thermography and optical tomography usage and compared it with micro–Computed Tomography findings on a 10x10x10 mm sample. They were able to find 71% of pores. [21]

Colosimo and Grasso criticize optical methods for only concentrating on the surface and not concerning about the physical phenomena occurring below the layer. They also criticize the lack of necessary sensors for “optical tomography” and the high-level (gigabytes) of data transfer needed for these methods [25].

There are only a few studies about in-process monitoring of L-PBF process by eddy current technology. Primary efforts are made by Todorov et al. They have reported promising results for 32 element array probe tests on Inconel 625 (In625), duplex stainless-steel 2205 (St2205), and carbon-steel 4140 (St4140) materials [26], [27].

Chapter 3

THE PROPOSED METHOD

3.1 Non-Destructive Testing Methods

Non-Destructive Testing is a general name for testing a component/part/equipment without causing damage to the part and using physical methods such as sound wave propagation, high power electromagnetic radiation transmission, capillary movement of fluids, etc. X-Ray radiography, Computational Tomography (CT), Fluorescent Penetrant Inspection (FPI), Magnetic Particle Inspection (MPI), Ultrasonic Testing (UT), and Eddy Current Testing (EC) are the basic NDT methods used by aerospace part manufacturers.

3.2 Eddy Current Testing

Eddy Current Testing is a surface and subsurface non-destructive inspection method. This method is applicable to conductive parts. **Figure 3.1** & **Figure 3.2** shows the basic physical interaction of the inspection process. An alternative current passing through a coil produces an alternating magnetic field. When a magnetic field penetrates a conductive material, within material, eddy currents occur as a reaction to the magnetic field. Eddy currents produce magnetic fields opposing the coil’s magnetic field [28].

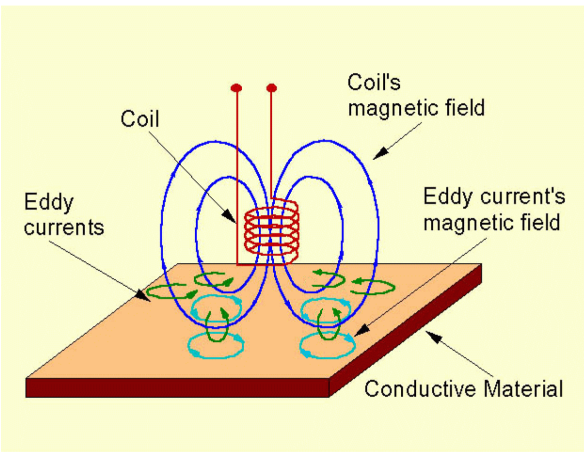

Figure 3.1 Coil's magnetic field and conductive material's response.[28]

These eddy currents vanish as the depth increases towards conductive material. The standard penetration depth is defined as 1/e or 37% of the surface density and changes opposite to frequency, material conductivity, and magnetic permeability. [29]

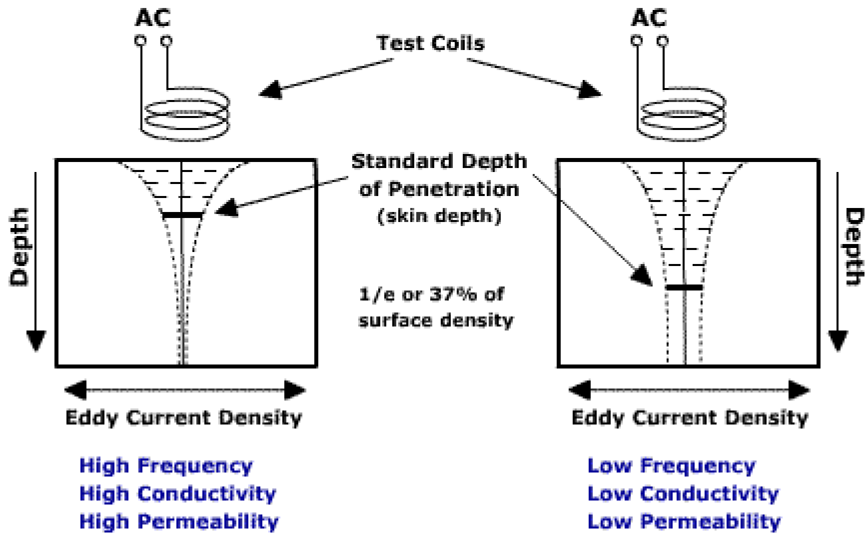

Figure 3.2 Eddy Current depth of penetration [29]

The formula for calculation of the standard depth of penetration is given below [29]:

$$\delta = \frac{1}{\sqrt{\pi f \mu \sigma}}$$

Where:

δ : Standard Depth of Penetration (m)

f : Frequency (Hz)

μ : Permeability (H/m)

σ : Conductivity (S/m)

As seen from the above formula, the penetration depth can be adjusted by changing the coil's frequency since the material's permeability, and conductivity cannot be adjusted during the inspection.

When the inspection coil is moved along the surface of the specimen, the eddy current response affecting the sensor coil can be seen on the impedance plane, as shown in Figure 3.3.

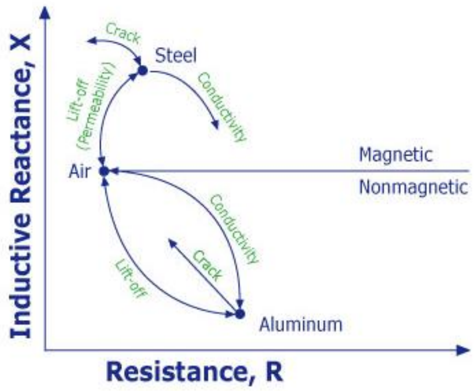

Figure 3.3 Eddy Current Impedance Plane Responses [30]

In the impedance plane, probe lift off, crack, and conductivity changes have different paths. When inspectors follow up on these responses, they can identify if the specimen has a defect or not. In automated inspection systems, these responses are collected synchronously to surface position to prepare surface eddy current response maps. Generally, when amplitude threshold limits are applied to these maps, the defects can be easily identified according to the position.

Main reasons and advantages for selecting Eddy Current inspection as an in-process monitoring and inspection method are:

- Working thicknesses are adjustable with frequency, and inspection thicknesses are very similar to L-PBF re-solidification thicknesses.
- Very sensitive non-contact inspection method.
- A matured and widely used inspection method for welds and L-PBF can be considered as a laser micro welding process.
- When compared to optic emission in-process monitoring methods, it does not observe the possibility of the defect during the process. It inspects the material and finds out directly the defect in the material.

On the other hand, the possible disadvantages are:

- The surface condition of L-PBF during the process is not as smooth as conventional production machined surfaces. This will cause additional noise and add features to eddy current responses, which can increase false positives and complicate the detectability of defects.
- For increased sensitivity, the inspection coil should be as close as possible to the surface. For L-PBF process, residual stresses or the wrong design of the build can cause a touch of the inspection coils. These kinds of contacts may damage the

build or inspection coils.

Besides the disadvantages, Eddy Current inspection method can be one of the most feasible methods for L-PBF in-process monitoring and inspection method.

3.3 ET Application as In-Process Monitoring/Inspection Method

First, the main reason for eddy current inspection to be taken as in-process monitoring and qualification system is the similarities between the physical depth of inspection penetration and L-PBF laser melting and re-solidification depth thicknesses. The measured melt pool re-solidification depth from metallographic cross-section images for the Inconel 625 L-PBF process is between 131.2-171.9 µm [11]. On the other hand, the standard penetration depth of eddy current inspection for 1, 2, and 3 MHz coil frequencies are 574, 406, and 302 µm for Inconel 625 material. As seen, all the important physical phenomena are accruing below half millimeters for both processes. ($\mu/\mu 0=1$, $\sigma=0.768$ MS/m [26])

Eddy current response is affected by material type, and temperature, microstructure, geometry, probe distance, probe type, frequency, environmental electromagnetic noise, electric system noise, digitization caused base noise, etc. If we assume the inspection system, inspection probe, and inspection frequency as constant, we can write the sum of eddy current response (shown as EC in the formula) in means of the sum of effecting variables as below formula;

$$\sum_{i=1}^{n} EC_i = f(EC_{geometry}, EC_{probe\ distance}, EC_{material}, EC_{microstructure}, EC_{noise})$$

If we assume environmental noise is very small in proportion to the eddy current signal. Eddy current signal is mostly based on geometry, probe distance, material, and microstructure variables. For a single position of EC probe, it is impossible to separate the response source. At least two probe position is needed to make a logical decision. For example, in manual conventional eddy current inspection, it is possible to identify small geometrical change (such as a crack) by moving the probe to a crack position from no crack surface and objecting a peak exceeding a threshold at the EC screen impedance plane.

As it is seen for conventional manual eddy current inspection, monitoring one signal value in a projected direction (generally vertical direction after calibration) is enough. On the other hand, eddy current data can give "direction" and "distance" information on the impedance plane, which consists of "Inductive Reactance" and "Resistance" axes.

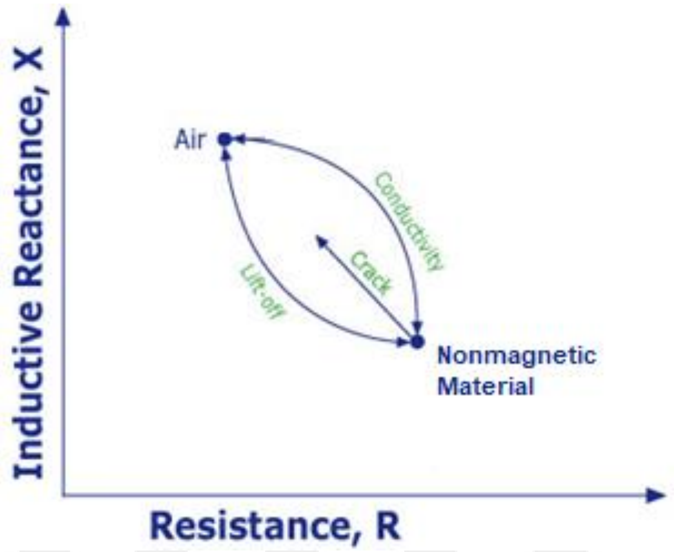

Figure 3.4 Impedance Plane and responses (After [30])

Eddy current data collection points for one coil of an array probe are shown below:

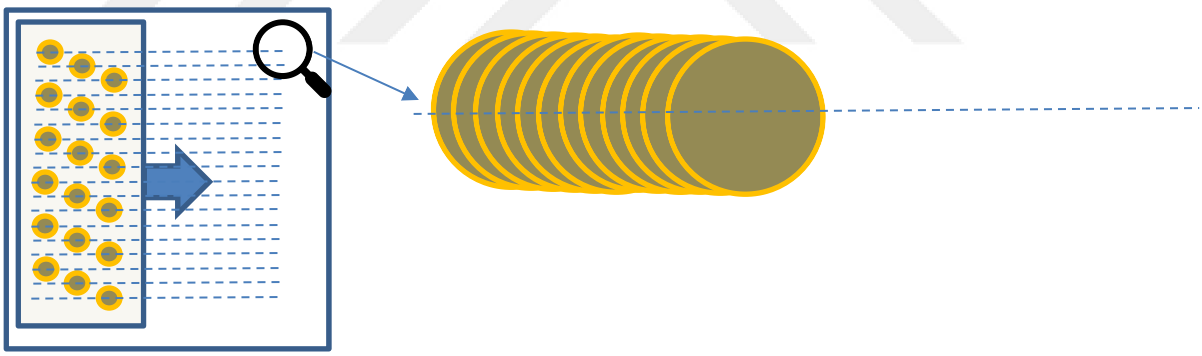

Figure 3-5 Array probe scan direction and one coil discrete data collection positions for surface coverage.

As seen from the above figure (left), the arrangement of coil positions on the array probe assures the surface coverage when the probe is moved to the right. EC data is collected and stored sequentially for each coil during this movement. Also, the above figure (right) shows a coil that is making point inspections with equal distances along its path.

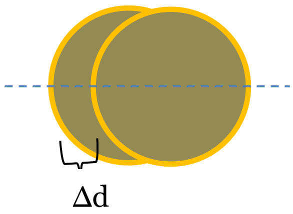

Figure 3.6 Two consequent probe positions with Δd distance

As shown in the above figure, if a coil is moved Δd and two eddy current responses are collected, they will have ΔEC difference in the impedance plane. If noise is assumed negligible, this ΔEC difference will also cover geometry, probe distance material, and microstructure caused differences.

$$\Delta EC = \Delta EC_{geometry} + \Delta EC_{probe\ distance} + \Delta EC_{material} + \Delta EC_{microstructure}$$

When an eddy current instrument can give high noise to signal ratio (negligible noise) and high-resolution eddy current response data, these minor differences can be used to identify defects with higher confidence.

The defect detection process can have two approaches; the first one is a deterministic approach, and the second one is Artificial Intelligence.

The deterministic approach uses basic mathematical algorithms that can be developed by correlation, regression, and the least square method on error minimizing, etc. It is a blind, direct, and conventional way of defect detection. Find out limit excess points, calculate area, and calculate a proportional response value to possible defect size.

On the other hand, artificial intelligence is one of the state-of-the-art computation methods for complicated inputs and outputs systems. By giving the complex inputs and identifying the demanded inputs with the selection of suitable AI methods (such as neural networks), the system can possibly identify defects for unseen conditions. The main disadvantage of artificial intelligence is that computation logic is a multidimensional BlackBox. This BlackBox is an unknown which has been set up on taught conditions. When an untaught situation occurs, the output has a chance to be unlogical. This makes artificial intelligence untrustable and questionable for defect detection. Although artificial intelligence has great potential and future for defect detection, it still needs some more time to gain trust. In this manner, artificial intelligence computation is out of the scope of this study.

Chapter 4

THE SYSTEM FOR APPLICATION TESTING

4.1 Overview of Test System

The test system consists of; a manipulator, a manipulator control device, test samples, and a data collection system (eddy current system).

The probe is moved by a manipulator system and connected to a commercially available eddy current system (Ectane 2 of Eddyfi), which provides two ±10 V digital readings for the vertical and horizontal axis of the eddy current impedance plane.

Horizontal and Vertical data are carried to the computer and recorded using the Magnifi software of Eddyfi.

4.2 The manipulator

The manipulator is a two-axis cartesian system moved by ball screws that are powered by stepper motors (Figure 4.1).

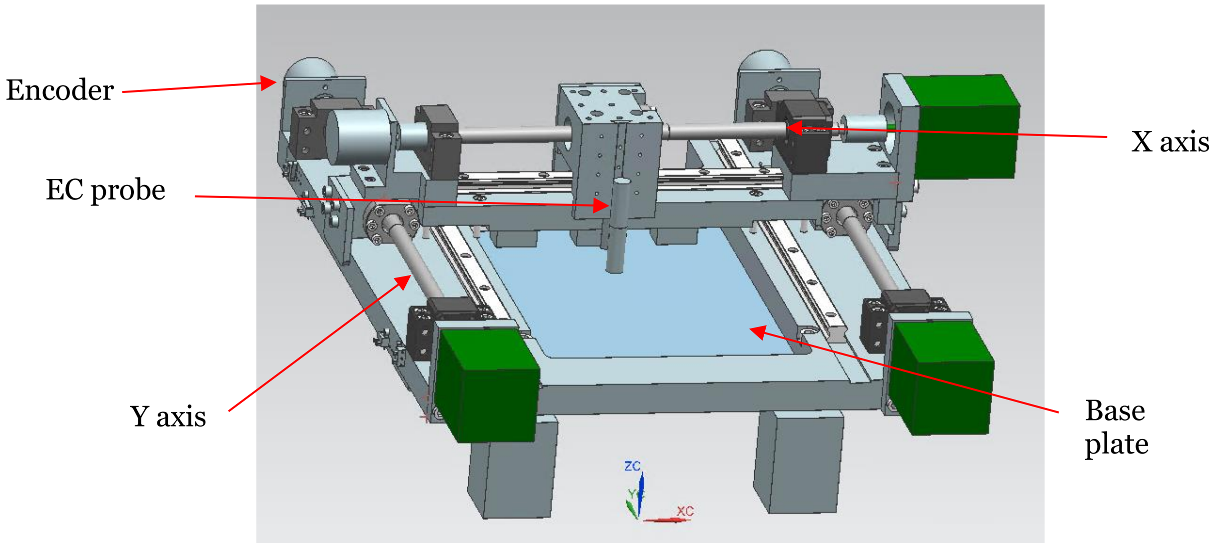

Figure 4.1 The manipulator system (fixed to base plate)

The eddy current probe is fixed to the X axis, which is carried by Y-axis ball screws. The height of the probe is adjusted and fixed manually on the calibration block, and during the inspection, it is not changed to the same concept as the eddy current array probe.

The reason for running the Y axis on two ball screws is to maintain accuracy during the inspection. All axis ball screws are connected to stepper motors on one side and encoders on the opposite side. The encoders supply actual probe position information.

4.3 Manipulator Control System

A control system drives the manipulator, consisting of 3 stepper motor drivers and an Arduino Mega for pulsing purposes (Figure 4.2). Move commands are sent from the Raspberry Pi computer, and the Arduino Mega board sends a necessary number of pulses.

Manipulator position readings are done by three encoders connected to the end of each axis screw mill rotated by the stepper motors.

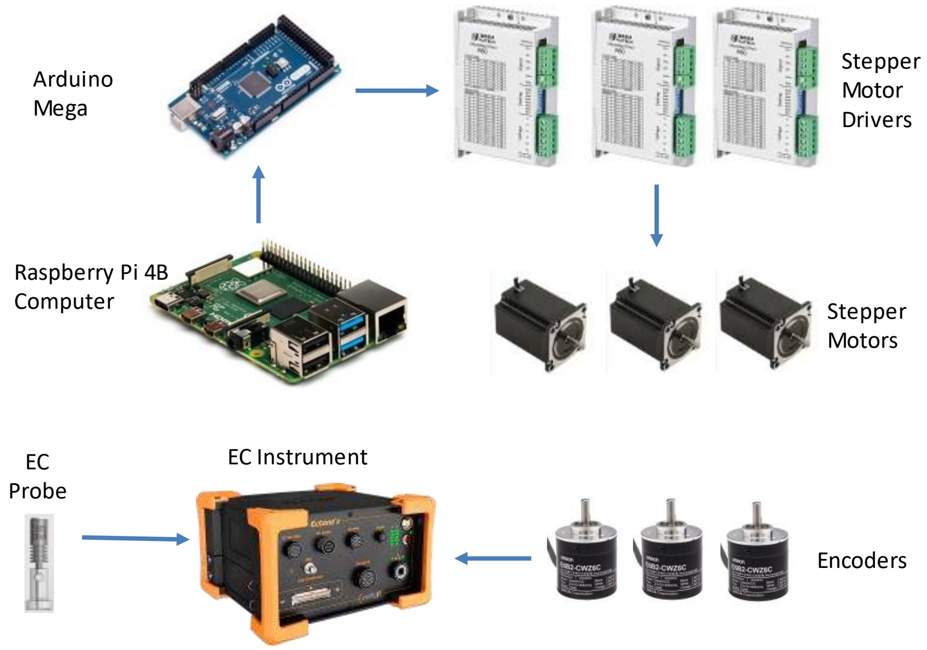

Figure 4.2 Illustration of manipulator control system

The probe's position is directly read from the encoders by the eddy current inspection instrument, Ectane 2. Both the position of the probe and eddy current signal data are recorded and sent to the computer.

4.4 Test Sample

The test sample is produced by the EOS M290 machine using Inconel 625 metal powder. An optimized production parameter set, and a purposeful bad parameter set are used for test parts' production. Each layer's thickness is 40 µm. Argon gas is used as the process gas. The optimized parameter set gives 99.96% relative density to bulk material, and the bad parameter set gives 17 % porosity relative to the bulk material.

The test sample is built on a C45 steel base plate. Various combinations of shapes are built as sample geometries. The geometries have slopes, curvatures, roundness, sharp edges, and flat top surfaces.

The test sample is based on the concept that calibration and inspection will be made on the same part. Dedicated defects at the top surface of the calibration blocks are used for calibration purposes. The main reason for integrating calibration defects to the test sample is to assure the same inspection clearance from the eddy current coil to the calibration surface as the same as clearance from the eddy current coil test sample top surface

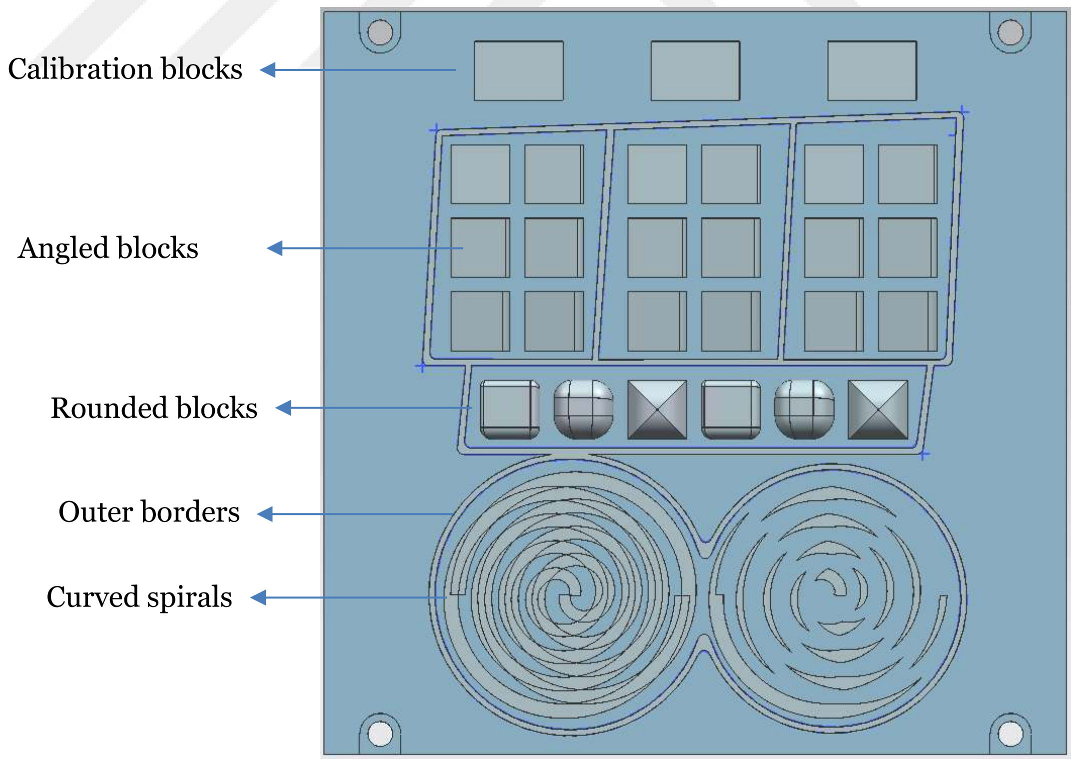

Figure 4.3 Illustration of test sample

The test sample consists of six different geometries, as seen in

***Figure* 4.3**. Calibration blocks, angled blocks, rounded blocks, two curved spirals, and outer borders.

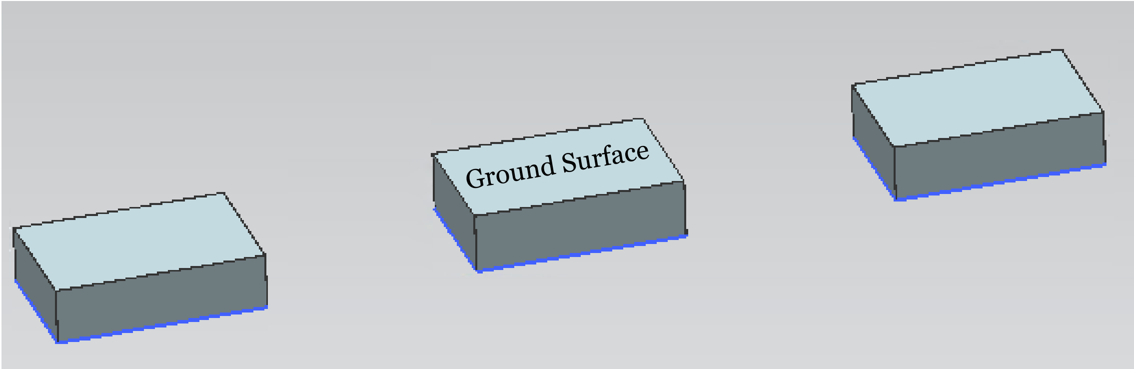

Figure 4.4 Illustration of calibration blocks

The calibration block set shown in Figure 4.4 consists of 3 rectangular prisms for calibration and data collection purposes. The middle block has a ground top surface. The grinding process decreased the surface roughness Ra from >7.5 µm to 0.36 µm. It is free of L-PBF process-related surface roughness and intends Eddy Current system calibration. The right block is for data collection purposes and has the same size 4 defects as the middle block. The left side block has 8 shallower defects and an L-PBF process-related rough surface.

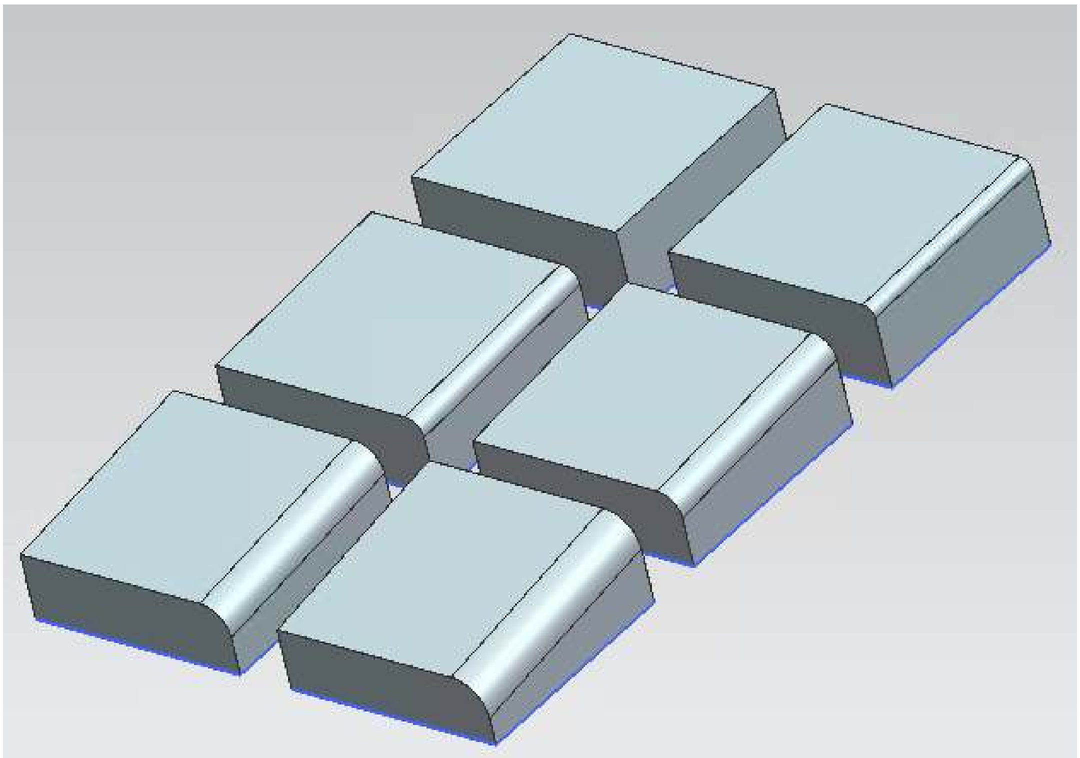

Figure 4.5 Illustration of sloped blocks

The sloped blocks shown in Figure 4.5 are varied rate sloped blocks with different radius edges on the right sides. The purpose of this group is to investigate eddy current response with slope and probe-material distance. The sample part has three repeating sets of sloping blocks, as seen in *Figure 4.3*. A bad parameter set is used for the third (right side) sloped blocks. They are assumed as the bad product of the laser system, and their expected porosity is ~17%.

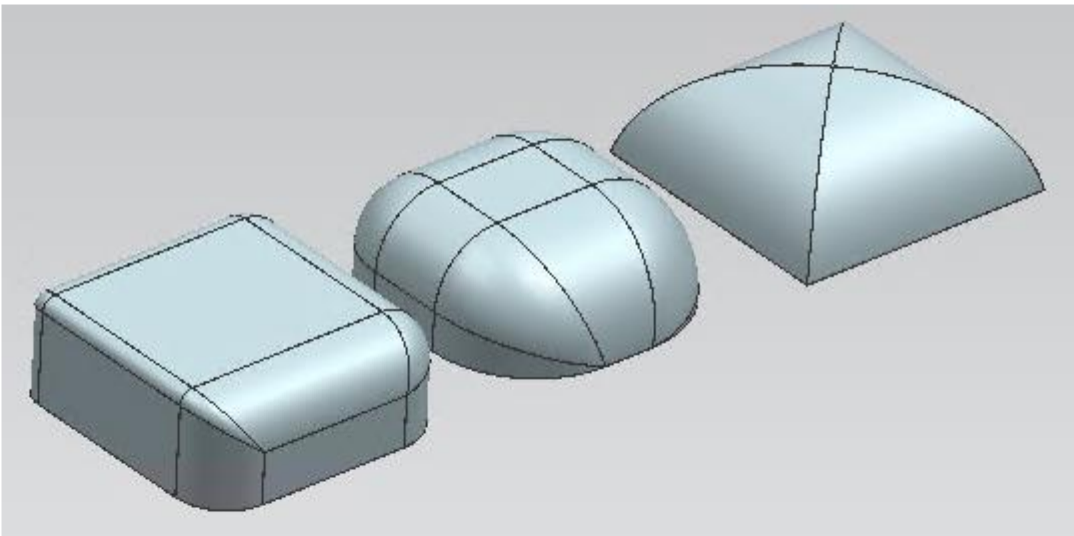

Figure 4.6 Illustration of rounded blocks

The rounded blocks shown in Figure 4.6 have rounded edges on all edges. These blocks' purpose is to investigate the eddy current data response on various site-rounded objects.

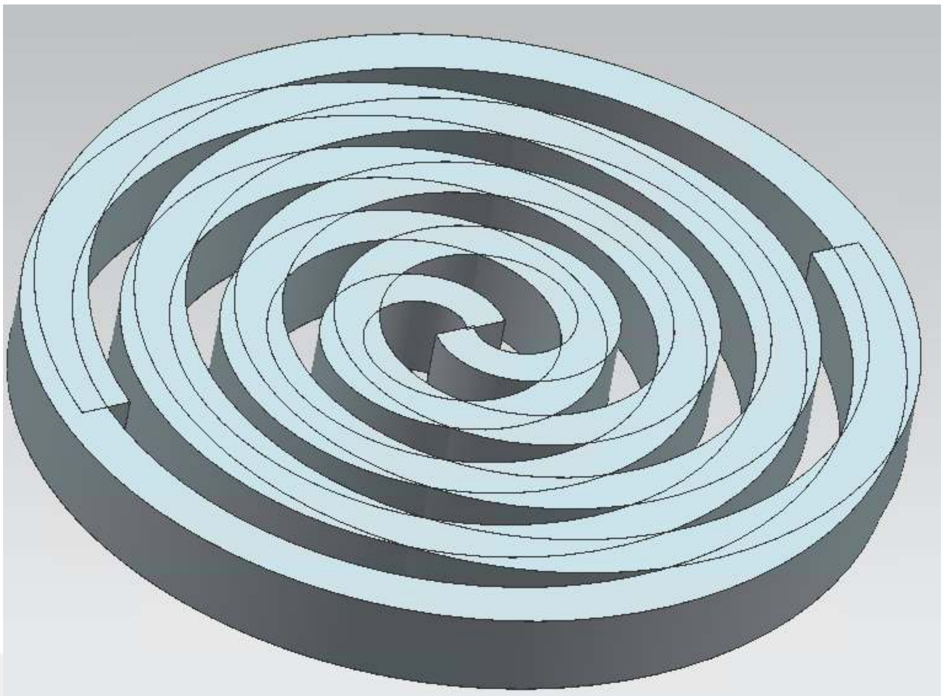

Figure 4.7 Illustration of curved spiral-1

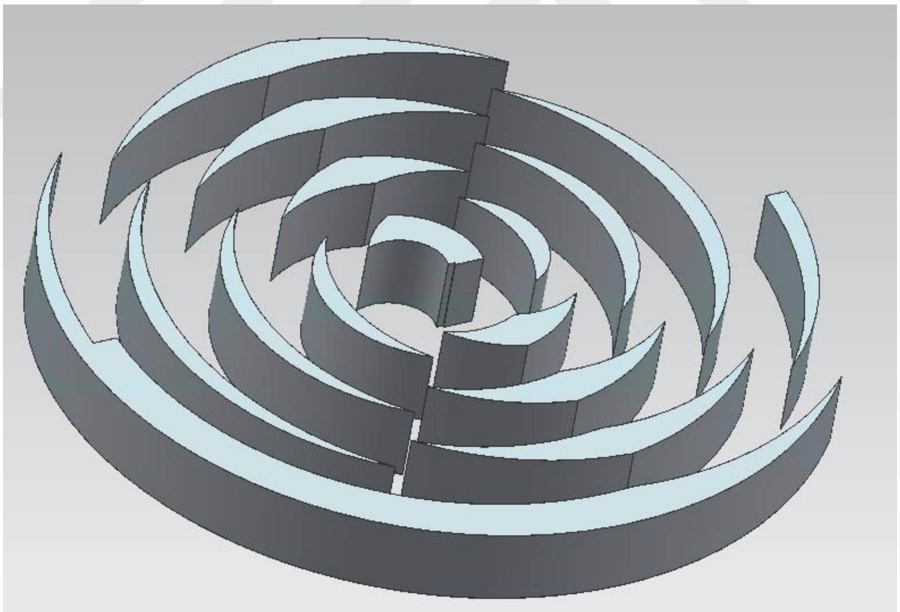

Figure 4.8 Illustration of curved spiral-2

The curvatures obtained by spiral shapes are shown in Figure 4.7 and Figure 4.8. They are aimed to analyze sharpness and radius effects on eddy current data.

In addition to the above shapes, external borders surround all the shape groups. External borders are built to hold the metal powder around the sample shapes during the eddy current data collection.

One crucial point about the test sample production is the usage of the "upskin" function. The upskin and downskin functions are used to get better surfaces at the up and down surfaces of the 3D parts, as shown in *Figure 4.9*. As it is stated in the previous sections, the study is aimed to give results of an in-process monitoring method. As a result, the test sample is also produced as an unfinished build process. In this manner, the upskin function is used for the upper surfaces except for the few layers of the top height.

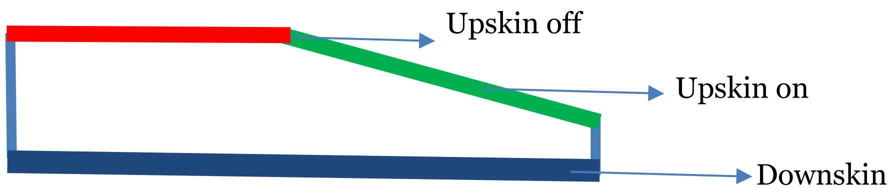

Figure 4.9 Illustration of Upskin and Downskin

The maximum built height of the test sample is 8 mm. Upskin function is disabled for the few layers of upper surfaces close to 8 mm.

The additively manufactured test part view after powder removal is shown in Figure 4.10.

Figure 4.10 Additively manufactured test part.

A critical thing for eddy current inspection is the calibration. Commercial calibration blocks are similar or the same as inspected materials with known size defects. It is difficult to find similar micro-structured additively manufactured calibration blocks since microstructure changes with additive manufacturing parameter sets. Calibration defects are built on the test part to minimize microstructure variability.

Calibration defects are machined to the test sample's calibration block areas. Despite other defects, calibration defect surfaces are ground to eliminate eddy current noise that would be coming from rough surfaces. Calibration block heights were given intentionally higher than other areas to balance the level with the remaining features after the grinding operation.

The deviation of optically measured surface dimensions with the CAD model of the additively manufactured test part is shown in Figure 4.11.

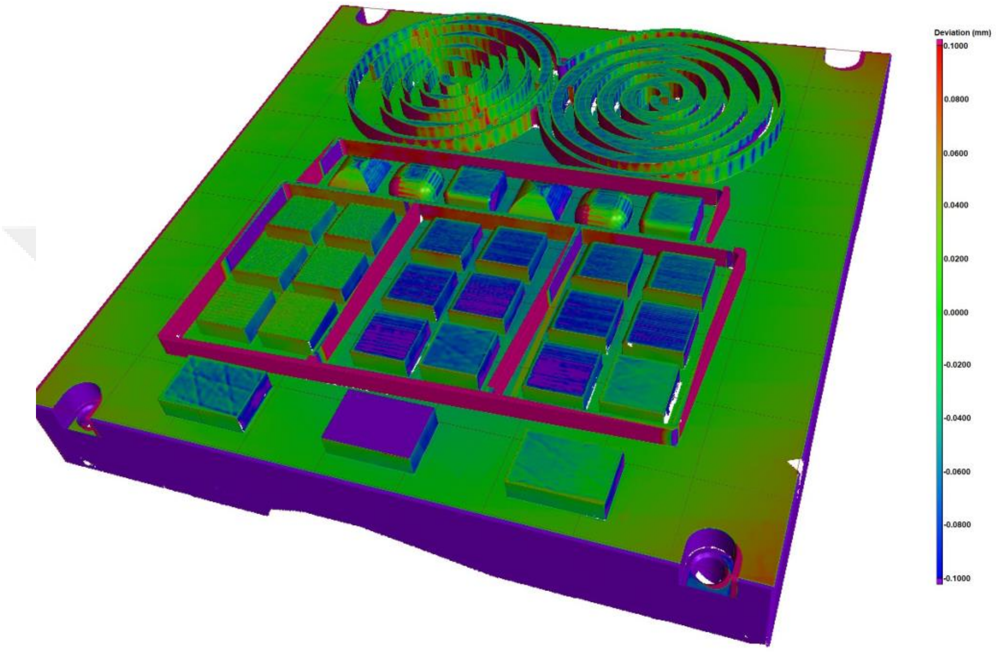

Figure 4.11 Additively manufactured test part, optical measurement.

4.4.1 Defect implementation system

Although the test part is composed of real production surface characteristics, it lacks known defects for inspection evaluation. As a rule of thumb, a defect is an unwanted discontinuity in material mass, decreasing mechanical properties. Additive manufactured parts contain a variety of defects like lack of fusion, porosity, and cracks. Defects can occur due to wrong manufacturing design/placement, powder conditions, bad parameter set, residual stresses, coater errors, laser system or manufacture system errors, environment, and more. Besides mentioned possibilities of defect causes, a water jet-guided laser system is used for defect manufacturing due to the higher controllability of defect sizes.

A water jet-guided laser system (or Laser microjet) is one of the state-of-the-art laser machining technologies. It uses a high-pressure, narrow water jet for carrying the laser beam to the work part surface (Figure 4.12).

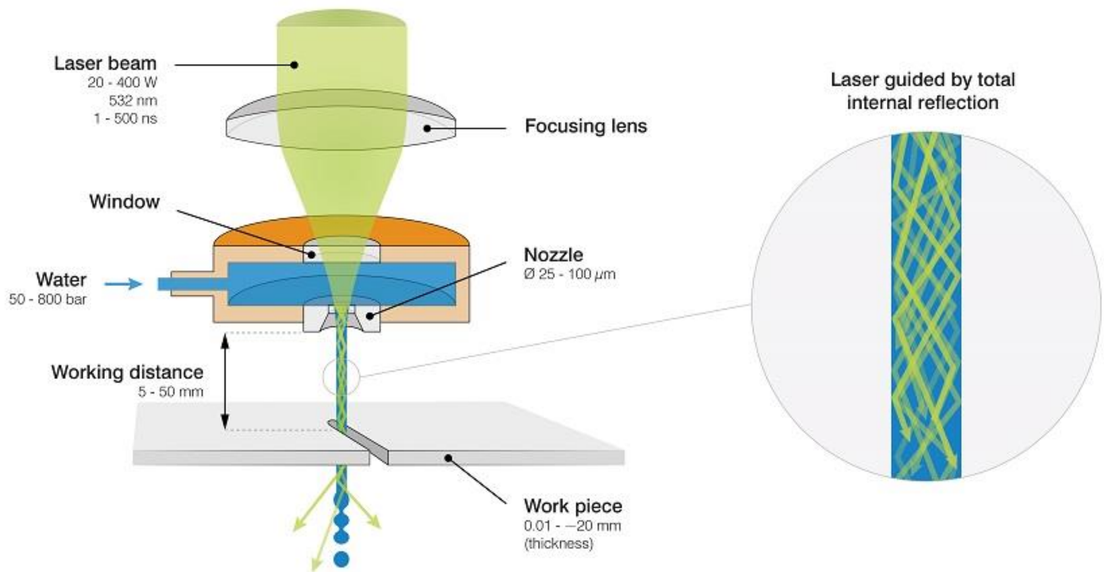

Figure 4.12 Water jet guided laser system (Synova) [31]

The main advantages of using a water jet-guided laser system are negligible heat effected and remelt zone occurs due to rapid water washing/cooling (Figure 4.13), and manufacture of high aspect ratio (depth/width) defects like Electrical Discharge Machining (EDM) are possible.

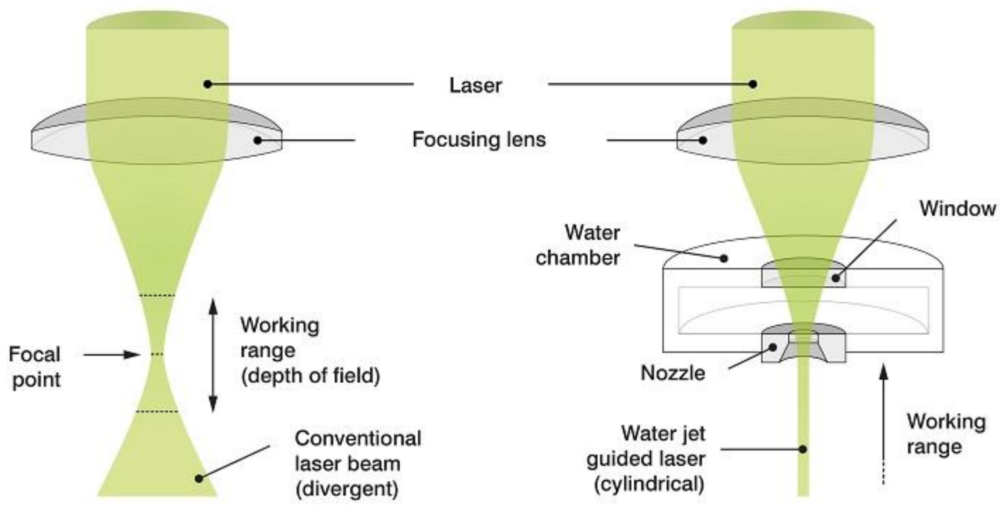

Figure 4.13 Left: Conventional laser beam, Right: Water jet guided laser beam [31]

After positioning the test part under the laser nozzle (Figure 4.14), defects are implemented using CNC code at once (Figure 4.15).

Figure 4.14 Synova MicroJet Laser system and test part

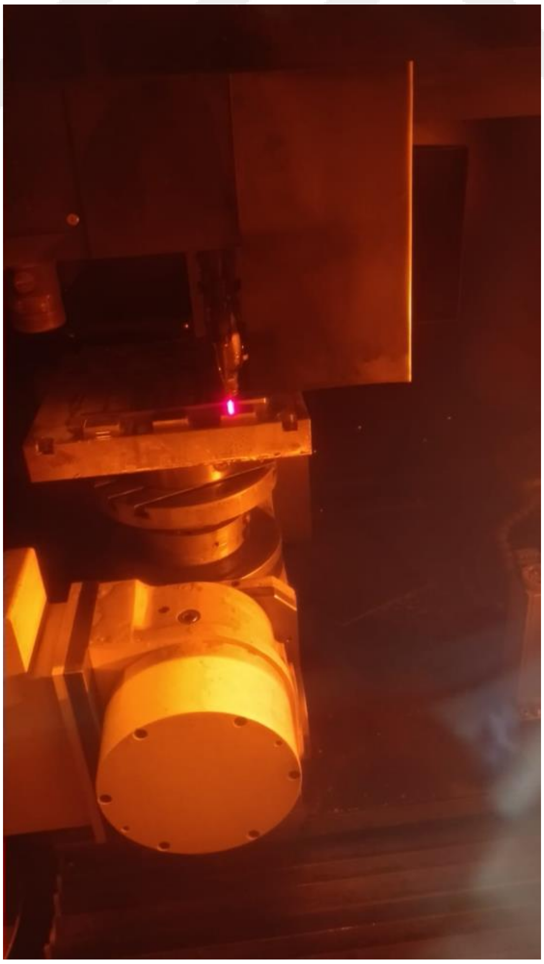

Figure 4.15 Synova MicroJet Laser system nozzle working on test part

4.4.2 Implemented Defects

Notch and hole types of defects are manufactured for evaluating the inspection capability. Notches and holes are the primary types of defects used for NDT methods for simulating discontinuities.

Test part notches are machined with two different definitions. The first one is a middle point given for coordinate location (Figure 4.17) , and the second one is located from the edge coordinate (Figure 4.16).

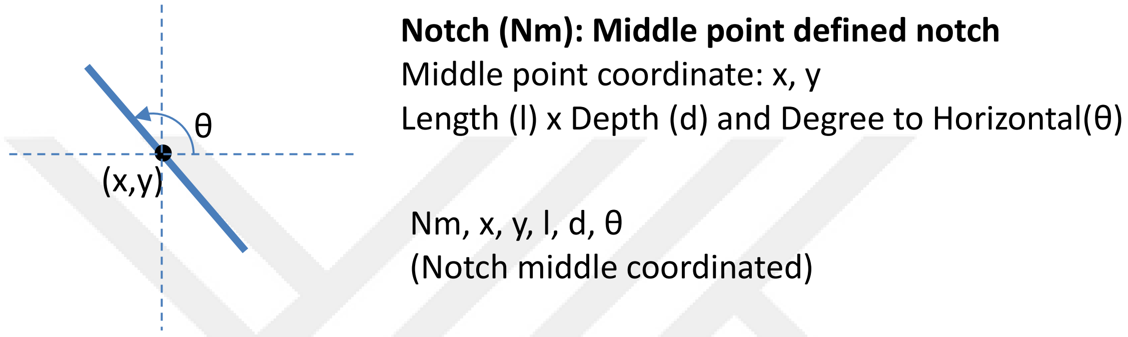

Figure 4.16 Middle point defined notch

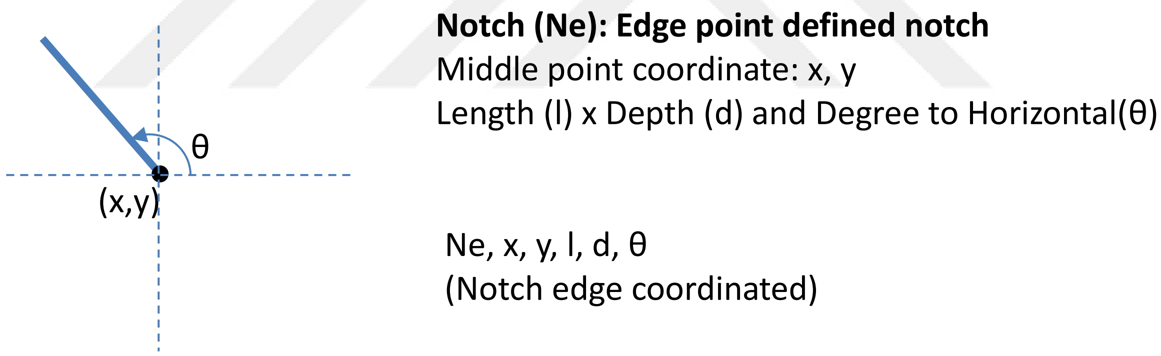

Figure 4.17 Edge point defined notch

Hole machining is based on center point location, diameter, and depth definitions (**Figure 4.*18***).

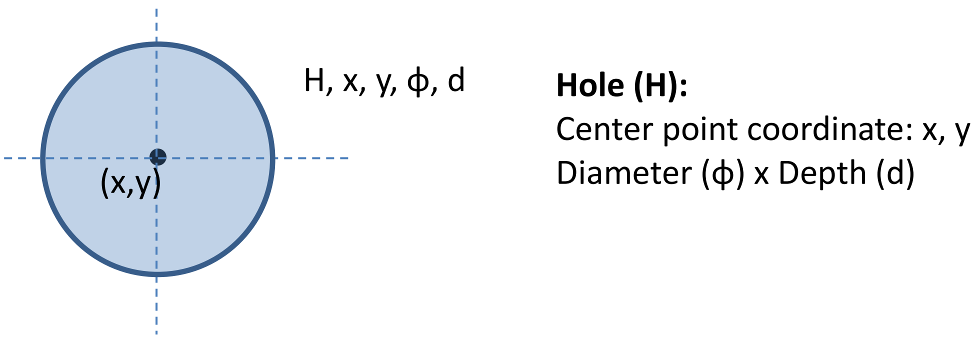

Figure 4.18 Center points defined hole

The edge of the middle rectangle prism is set as the origin point for positioning the defects (Figure 4.19).

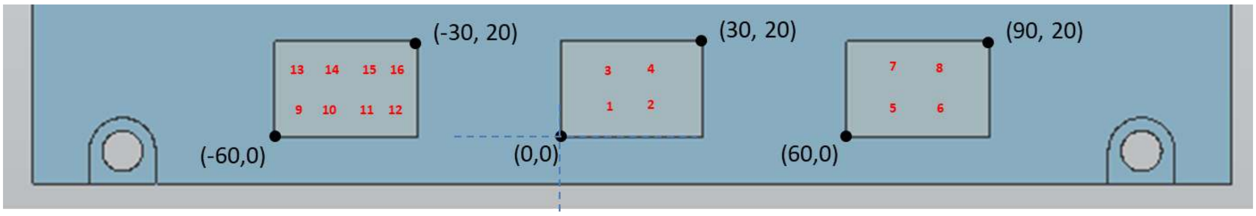

Figure 4.19 Defect numbers on blocks and coordinates

The defects are machined based on location (X, Y: mm) and characteristic parameters such as length (L: mm), depth (D: mm), angle (θ: deg), and diameter (ϕ: mm) (*Table 4.1*).

Table 4.1 Defect size and location table

Defect #	Defect Type	X	Y	L	θ	ϕ	D
1	Nm	10	7	0.75	90		0.375
2	Nm	20	7	0.5	90		0.25
3	Nm	10	14	0.2	90		0.04
4	Nm	20	14	1	90		0.1
5	Nm	70	7	0.75	90		0.375
6	Nm	80	7	0.5	90		0.25
7	Nm	70	14	0.2	90		0.08
8	Nm	80	14	1	90		0.1
9	Nm	-54	7	1	90		0.12
10	H	-48	7			0.4	0.2
11	Nm	-42	7	1	90		0.2
12	H	-36	7			0.3	0.2
13	H	-54	14			0.2	0.2
14	Nm	-48	14	1	90		0.08
15	H	-42	14			0.1	0.2
16	Nm	-36	14	1	90		0.04

The whole list of defect locations and illustrations of defect locations are given in Appendix A.

4.5 Data Collection

For data collection, Eddyfi's Ectane 2 Eddy Current instrument (Figure 4.20), Uniwest's pencil probe 2MHz PSR-.187 (Figure 4.21), designed manipulator, and control systems are used.

Figure 4.20 Eddyfi's Ectane 2 Eddy Current instrument

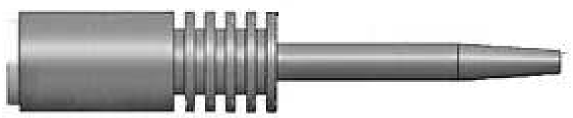

Figure 4.21 Uniwest's pencil probe with 0.750 mm diameter coil

Eddy Current data is collected with position information read from the manipulator system's (Figure 4.23) X & Y axis encoders (Figure 4.22).

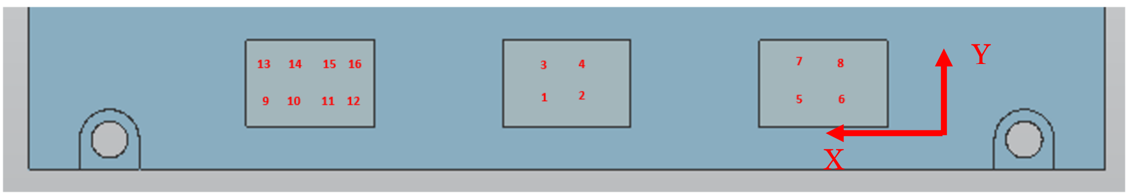

Figure 4.22 Defect numbers and data collection axes

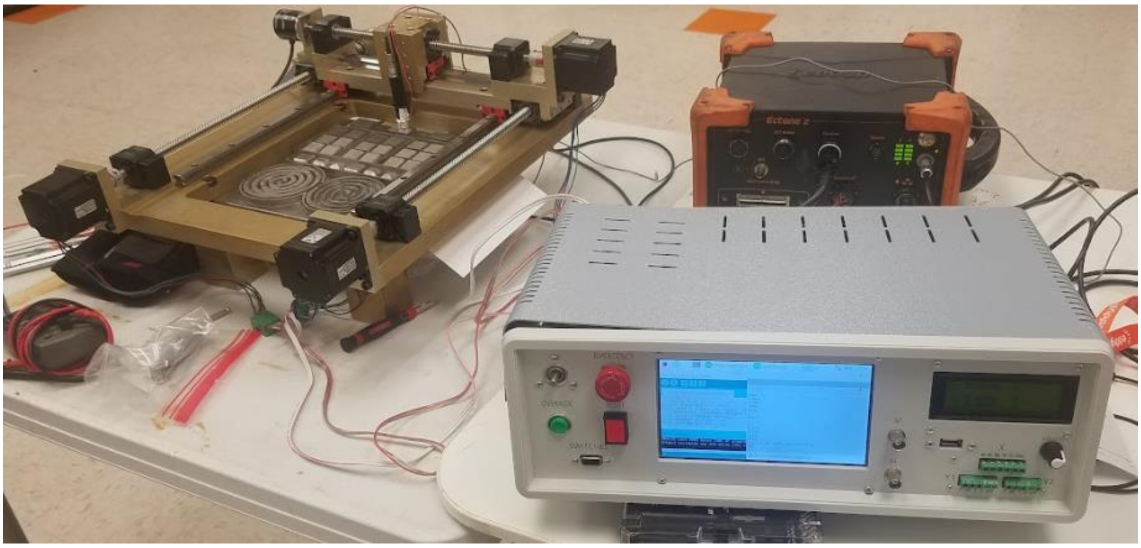

Figure 4.23 Data collection setup

C-scan image of the surface magnetic response is collected with Ectane 2 instrument, saved with the Magnifi software (Figure 4.24), and exported to .csv files for further numerical data analysis.

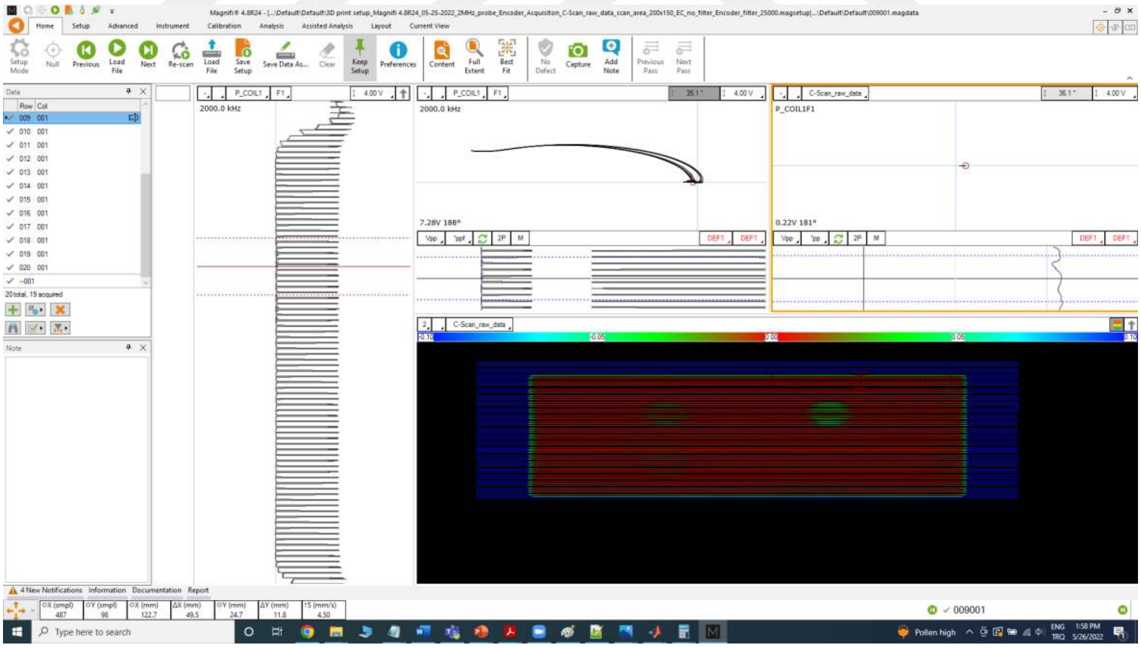

Figure 4.24 Magnifi software, Eddy Current signal and C-scan image screen view

Chapter 5

DATA ANALYSIS

5.1 Overview of Data Analysis

Data analysis and necessary computations are done in MATLAB and Python environments. The necessary eddy current raw data and probe positions are taken directly from Ectane 2's Magnifi software. The raw eddy current data is firstly exported to a .csv (Comma Separated Values) file to be taken into MATLAB as an array.

The eddy current data is affected directly by the surface condition. So, in addition to eddy current data, surface physical coordinate information is added to the analysis through the point cloud. Horizontal and vertical eddy current arrays and surface point clouds form the data mapping. The defect detections are completed with data analysis on MATLAB software Using these two arrays and one surface data.

5.1 Data Mapping

The data saved from eddy current scanning is a surface electromagnetic response map (also known as C-scan) type recording and exported to .CSV (Comma Separated Values) file (**Figure 5.*1***) to be able to make computational analysis.

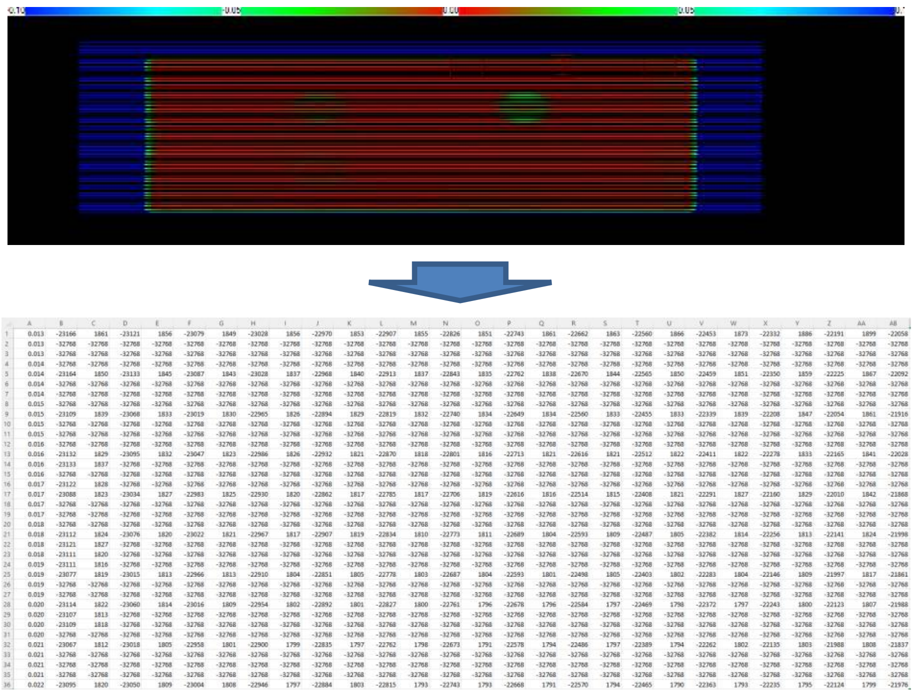

Figure 5.1 Magnifi software export to .CSV file

The .csv file's first column is the Y-axis positions of the probe, and the others are horizontal and vertical eddy current signal recordings, respectively, at each increment of the probe movement.

As is seen from the C-scan image, all the rows have some spaces between them because the incremental Y-axis movement of the probe is also recorded (vertical lines seen at both ends of the rows in Figure 5.1 colorful horizontal lines). First, the empty rows are cleared from the CSV data files.

After clearing the empty files, the eddy current .csv file is used to form 2 separate arrays of eddy current data for data mapping. The first one is the Horizontal Eddy Current data matrix, and the second is the Vertical Eddy Current data matrix. These arrays row and column elements correspond to the position on the eddy current probe, such as Figure 5.2 eddy current vertical array image.

Figure 5.2 Vertical Eddy Current Array image

In addition to Horizontal and Vertical Eddy Current data arrays, laser 3D surface scanning also provides valuable information for analysis. The eddy current inspection is affected by probe clearance or surface conditions. If surface conditions are known, these can be considered during analysis.

The sample material has 3D surface scanning data. Surface condition data is point cloud data obtained from the ATOS laser scanning system. The data file is enormous, and the points other than the inspection surface are unnecessary for analysis.

The volume of interest (Figure 5.3), which contains the analysis surface first filtered from the whole data, and the data size decreased (Figure 5.4).

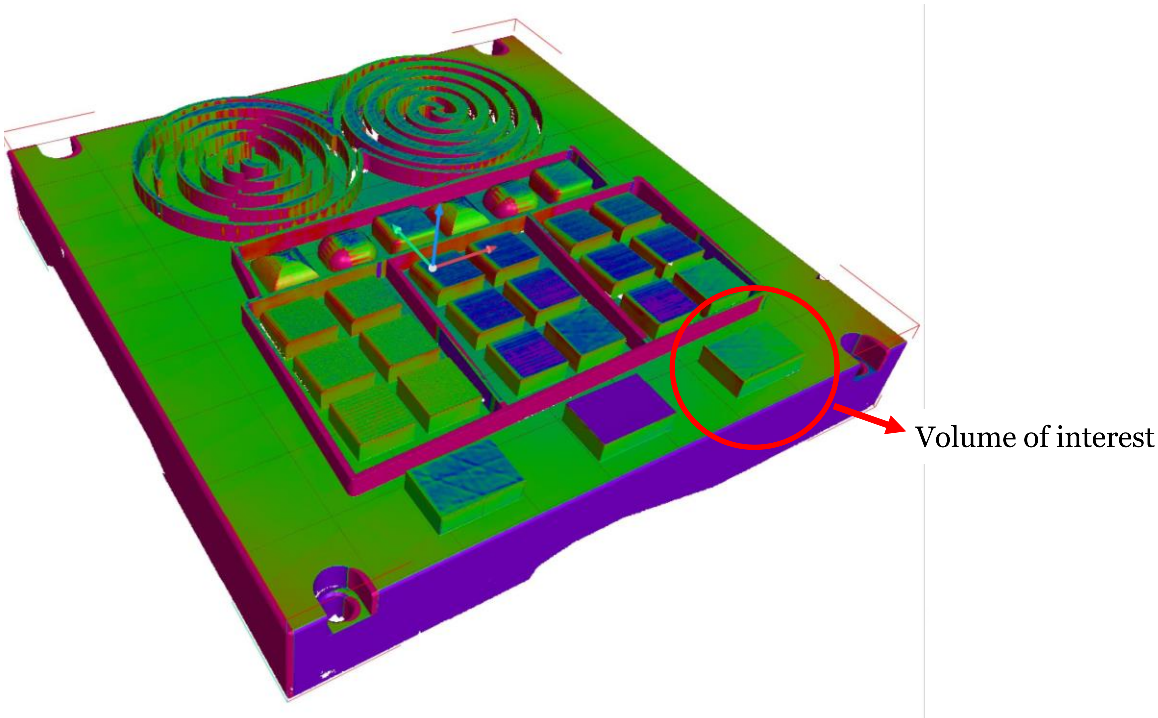

Figure 5.3 Volume of interest which contains the analysis surface

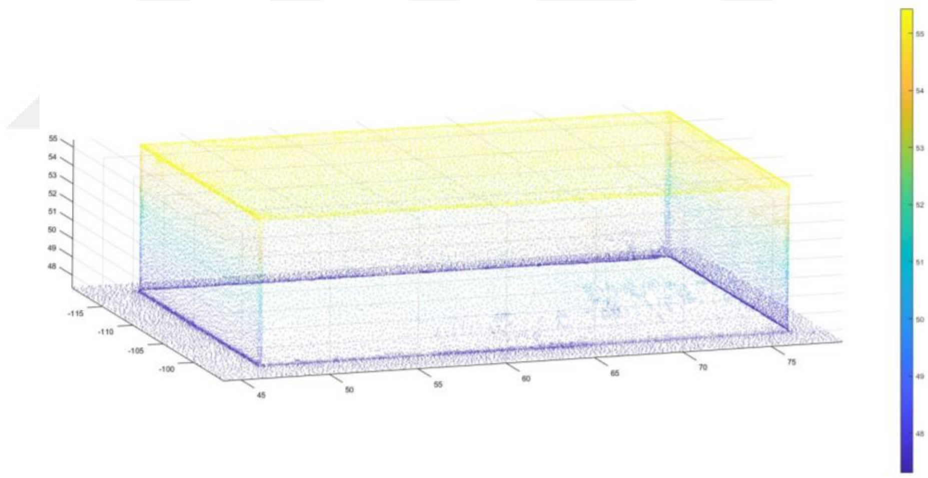

Figure 5.4 Decreased volume of point cloud containing the interested feature

For eddy current inspection, only the top surface and just a few hundred micrometers depths are essential, and the below is a blind volume for eddy current inspection. The point cloud at decreased volume still contains the baseplate points and prism edge surfaces which are not affecting eddy current data and are unnecessary for a benchmark.

In that manner, only the top surface and a few hundred microns from the edge surfaces should be benchmarked, as shown in Figure 5.5.

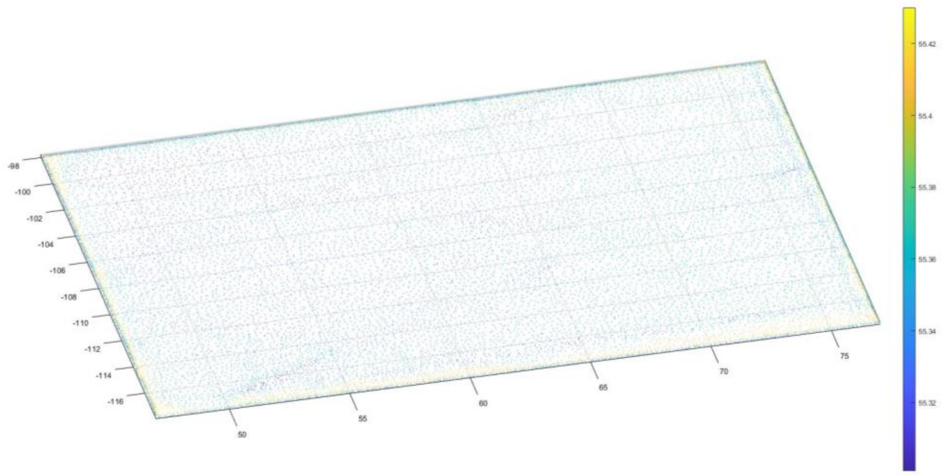

Figure 5.5 Top surface point cloud of interested area

Data mapping completes as Horizontal, Vertical eddy current arrays and surface point cloud of the arrays' location is collected.

5.2 *Defect Identification*

During eddy current data collection, the impedance plane angle is adjusted to show probe lift off as possible as the horizontal axis. Defect signal orientations should be assumed to be found on the vertical axis. This means defect identification analysis can be made using only vertical axis eddy current data.

The eddy current data collection was made on three blocks (Figure 5.6)

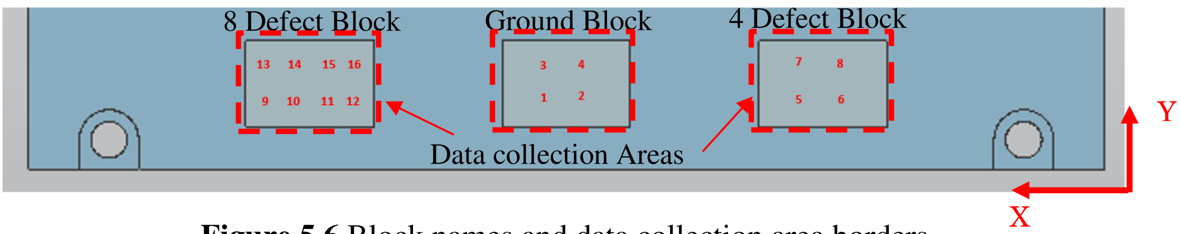

Figure 5.6 Block names and data collection area borders

Eddy current raw data values are shown according to data collection point numbers through Figure 5.7-Figure 5.9. At these figures, first seen peak values are caused by the edge effects of the eddy current signal. When the probe comes from air to material or material to air, it reads peak changes.

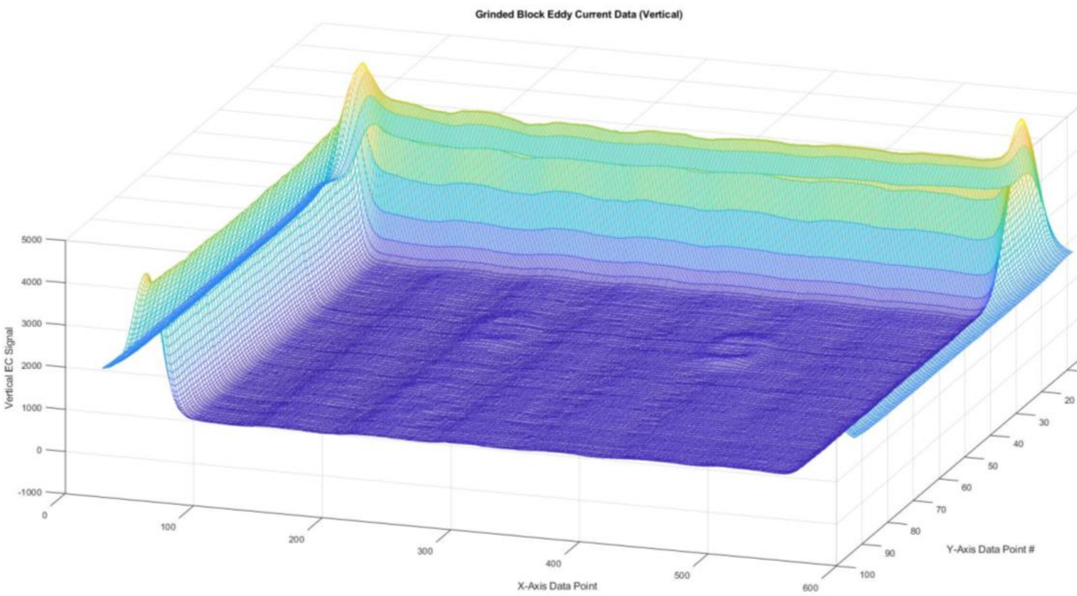

Figure 5.7 Ground block vertical eddy current data

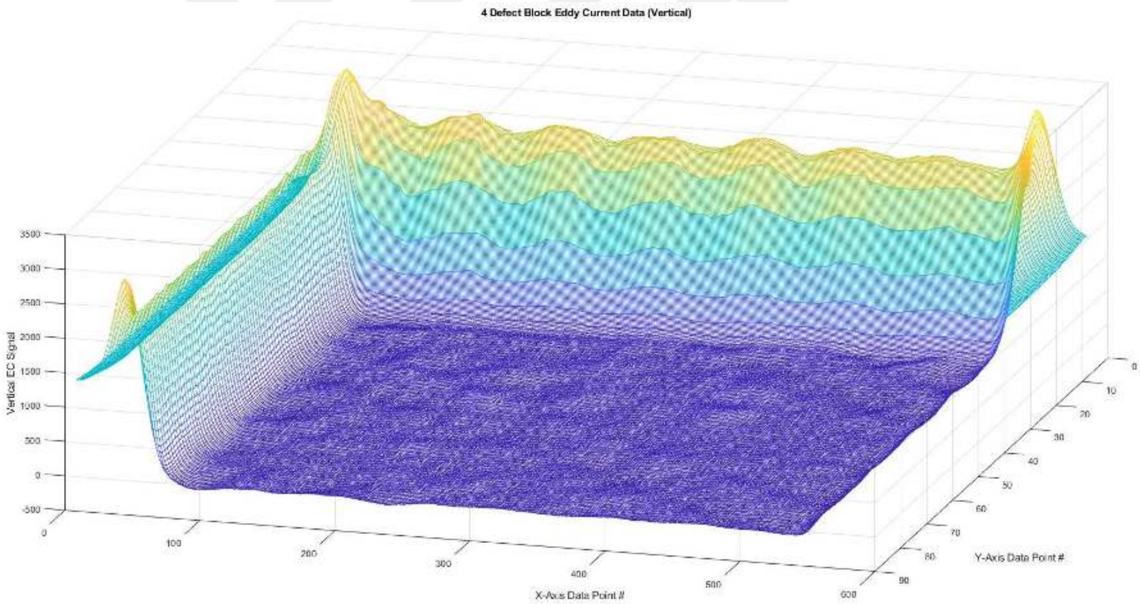

Figure 5.8 4 defect block vertical eddy current data

Since there are no defects at the edge sides, the signals coming from the edges can be eliminated. If there had been some intentional defects at edge sides, that analysis should be considered separately. The edge-separated images are shown through Figure 5.10-Figure 5.12.

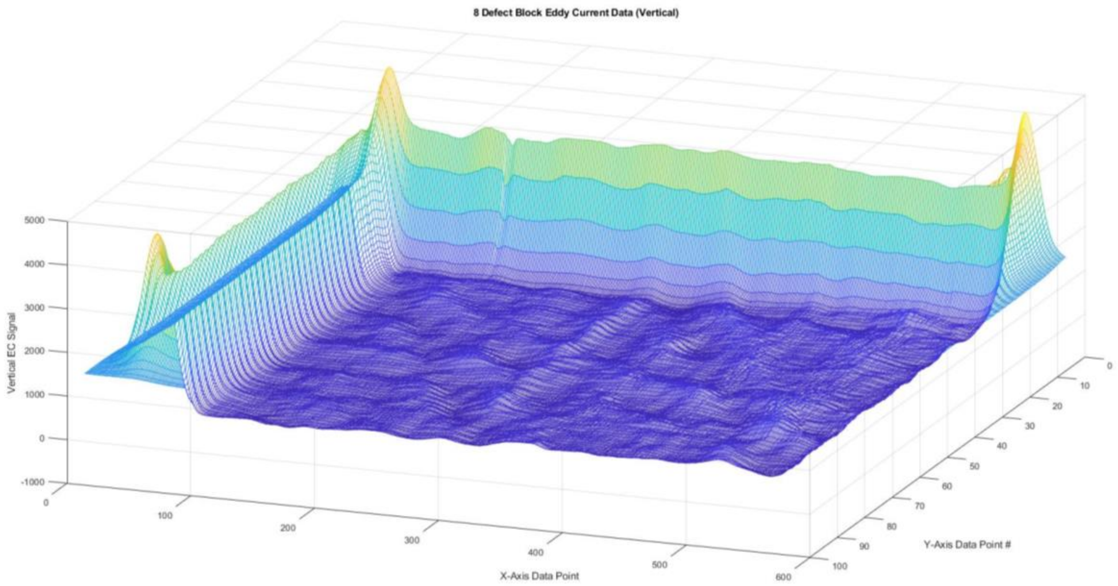

Figure 5.9 8 defect block vertical eddy current data

In Figure 5.10, the three defects can be identified easily, but the 4th one is not visible directly.

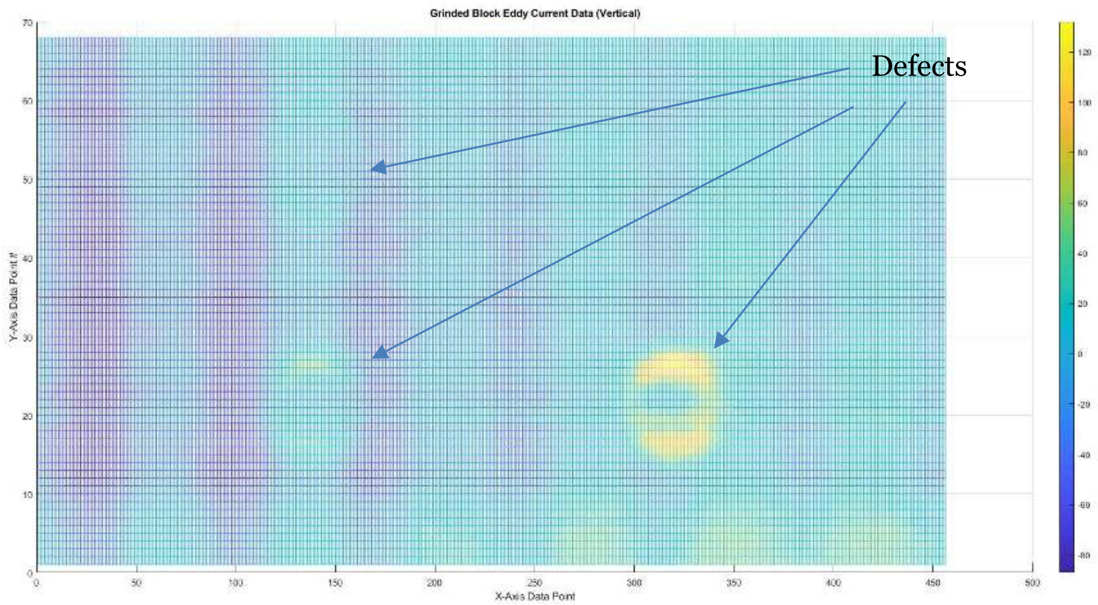

Figure 5.10 Ground block vertical eddy current data (edge effects excluded)

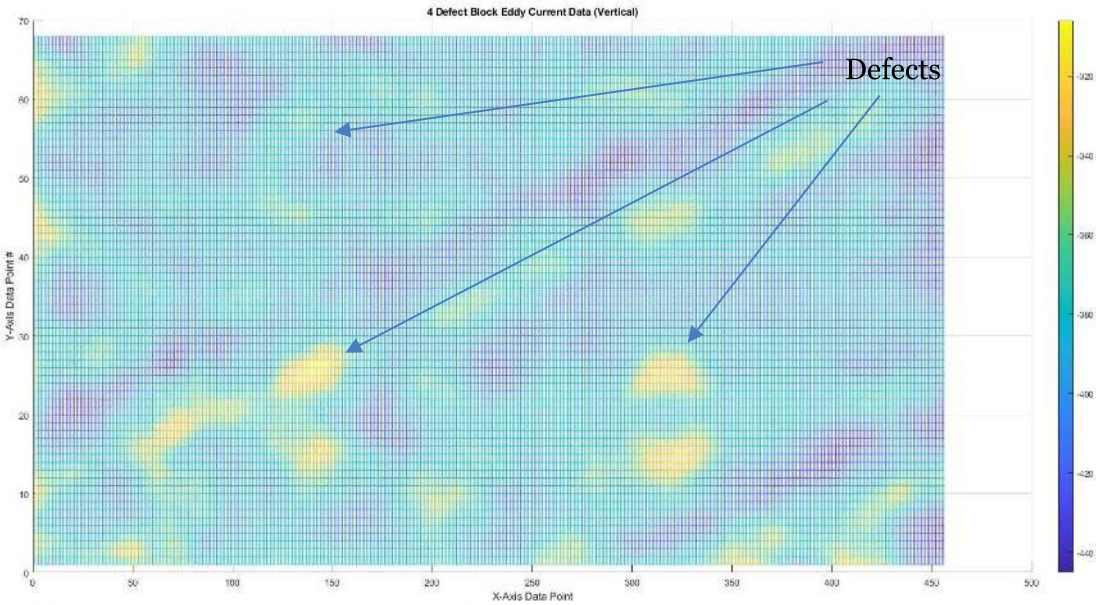

Figure 5.11 4 defect block vertical eddy current data (edge effects excluded)

In Figure 5.11, the three defects can be identified easily, but the 4th one is again not visible directly or not detected.

In Figure 5.12, eight defects are embedded, but none of them can be identified directly.

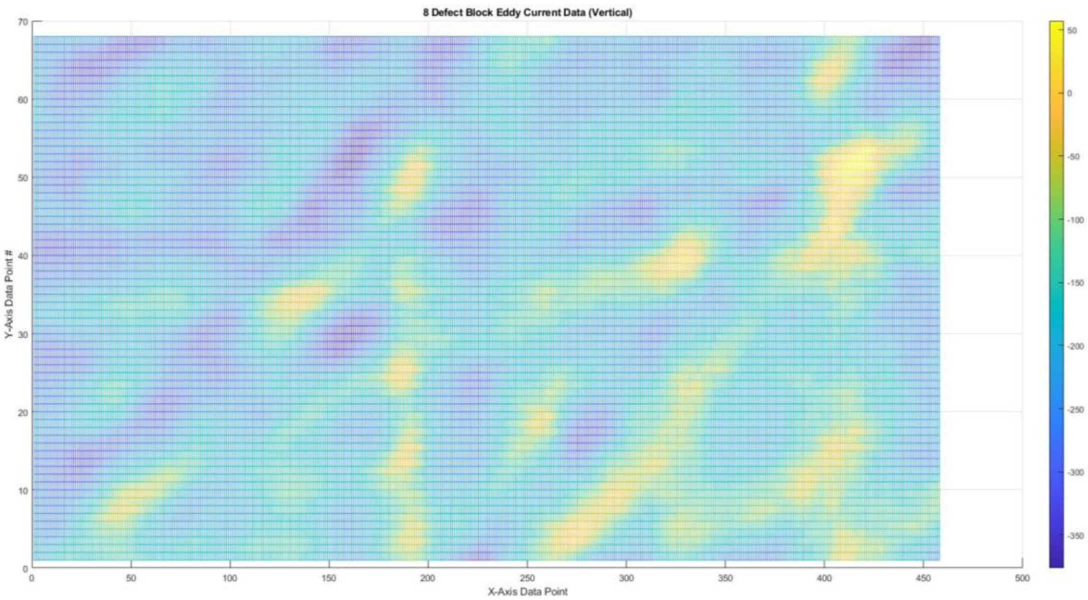

Figure 5.12 8 defect block vertical eddy current data (edge effects excluded)

When 4 defect and 8 defect blocks' eddy current signals are investigated from an isometric view, the waviness is found to be remarkable (Figure 5.13, Figure 5.14). This waviness can be caused by the rough surface of the L-PBF process. If the 3D laser scan surface data and eddy current vertical data are compared to each other, there are some similarities along the laser pathways that are visible (Figure 5.15 and Figure 5.16). The 3D surface laser scan data and eddy current data images can be compared for differences for easier defect detection. Still this kind of analysis needs much more complicated calculations and very precise location measurements on both systems.

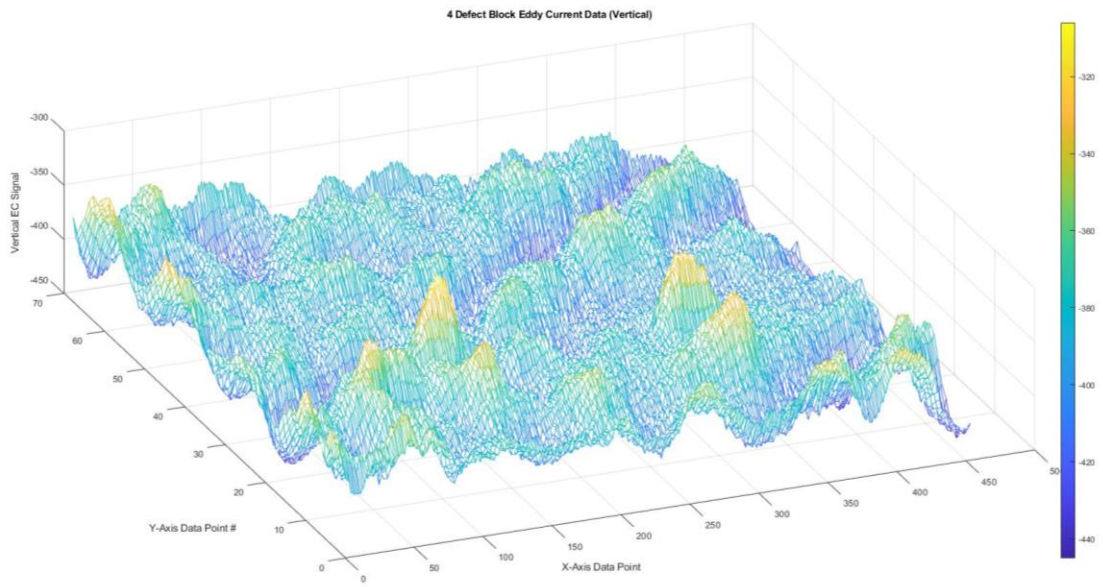

Figure 5.13 4 defect block vertical eddy current data isometric view

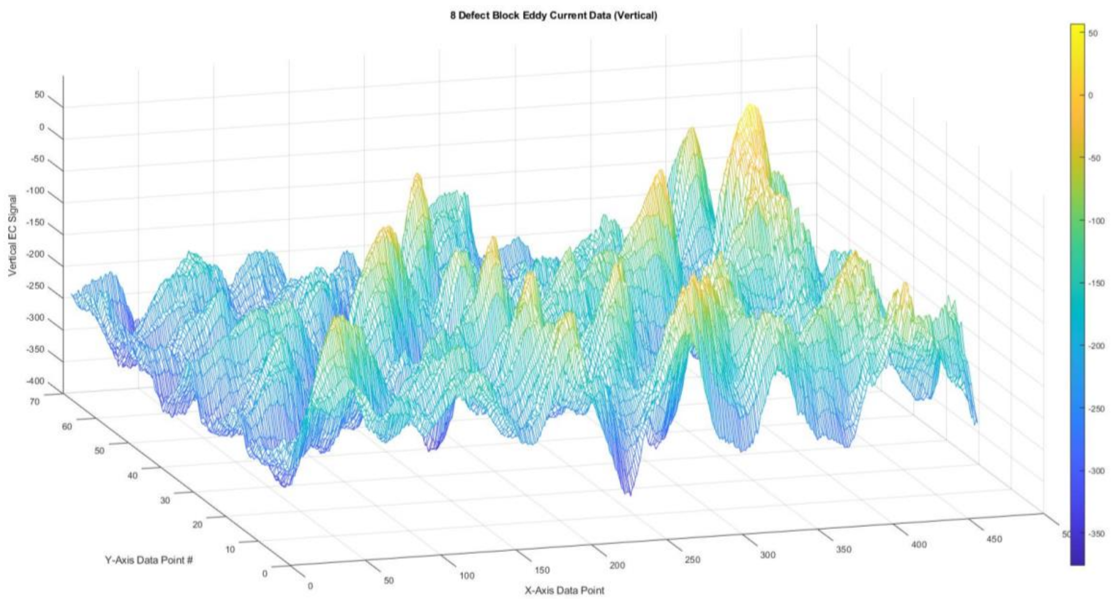

Figure 5.14 8 defect block vertical eddy current data isometric view

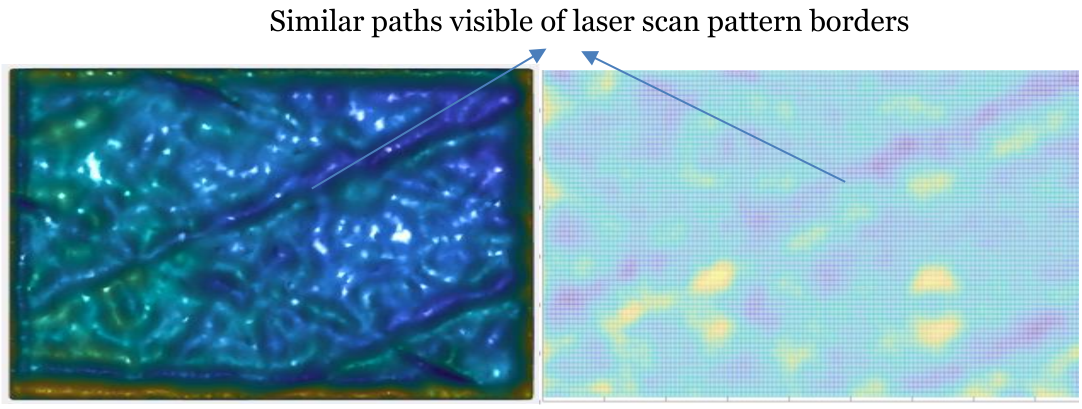

Figure 5.15 4-defect block; left: 3D laser scan point cloud X axis inverted according to EC scan direction, right: vertical eddy current data

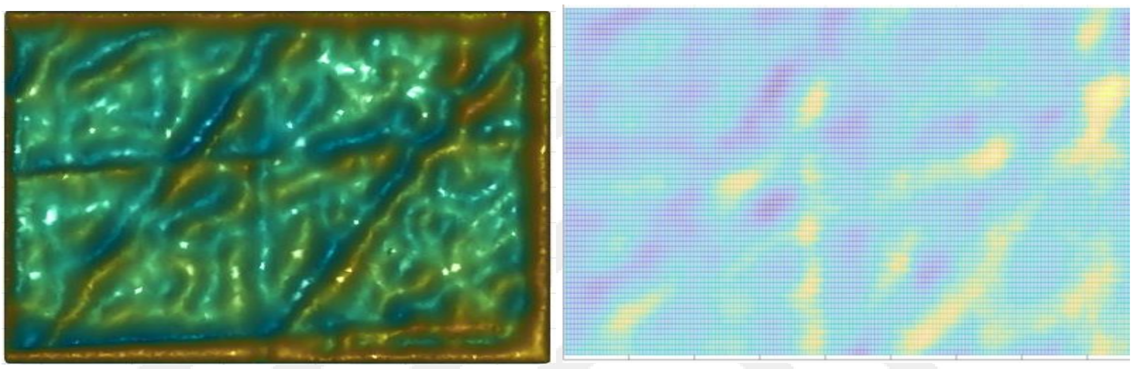

Figure 5.16 8-defect block; left: 3D laser scan point cloud X axis inverted according to EC scan direction, right: vertical eddy current data

Since the ground block has a smooth surface when compared to other blocks, a steadier signal is expected. But a waviness phenomenon is objected along the data collection X-axis (Figure 5.17). This waviness peak height is relatively high and comparable to defect peak signals. It can easily shadow small defects.

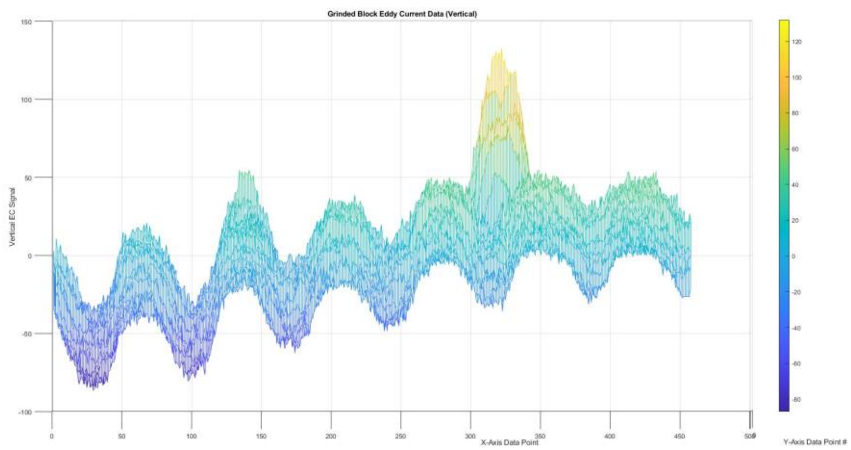

Figure 5.17 Ground block vertical eddy current data waviness view

Although firstly, the reason for the waviness is assumed to be microstructure caused, the orientation of the waves is not coherent with L-PBF laser scan paths. So, these extra eddy current signal waves could not be caused by microstructure or residual stresses.

The only logical explanation for the waviness phenomenon is eddy current probe vibration during motion. Even a tiny amount of vibration generated from the X-axis stepper motor or the rail or screw mill system can tilt the probe to micrometer levels and cause extra noise in the eddy current signal. The periodicity of the wave looks like occurring every ~4.4 mm

This kind of noise adversely affects the detectability of defects; however, this is a valuable lesson for future array probe designs for considering significant vibration effects for in-process inspections for the L-PBF process.

The best option for analysis of noisy collected data for correction is applying a filter. If 2-line samples (**Figure 5.*18***) are taken from ground block eddy current data (one is on defect path, one is no defect path), the FFT result will be as shown in **Figure 5.*19***. The possible vibration peak is at 0.47 Hz. The defect frequency signal peaks and the vibration frequency peak are very close, below 1 Hz. A high pass filter to decrease the noise level will probably reduce the amplitude of the defect signal also.

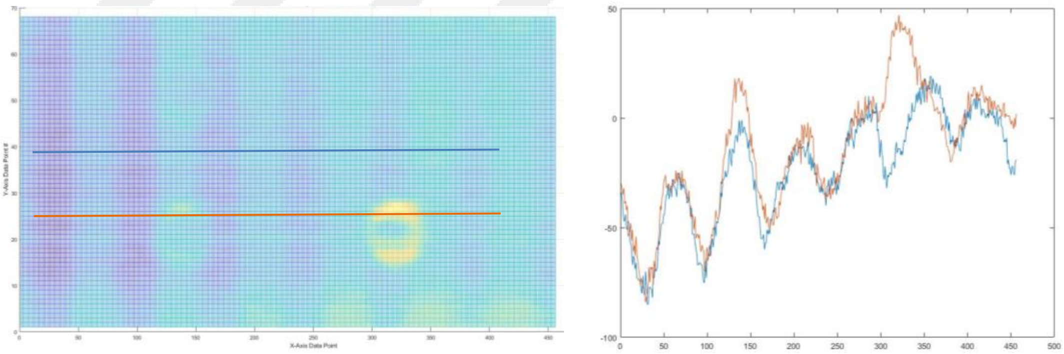

Figure 5.18 2-line samples taken for FFT analysis (defect on orange line)

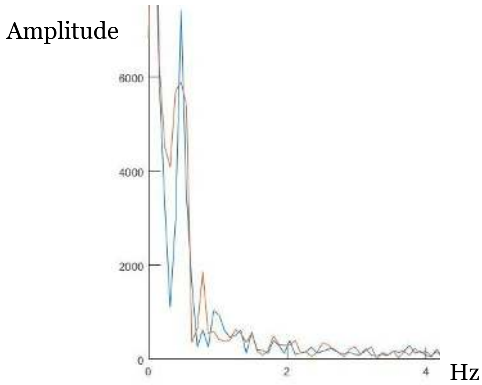

Figure 5.19 FFT analysis of defect path and no-defect path (defect on orange line)

If an FIR Equiripple High pass filter is applied to eddy current data, the image of the collected eddy current data changes through **Figure 5.*20*-Figure 5.*22***. As seen from the pictures, the effect of the waviness is decreased, but on the other hand, the amplitude and contrast differences of defects are also decreased.

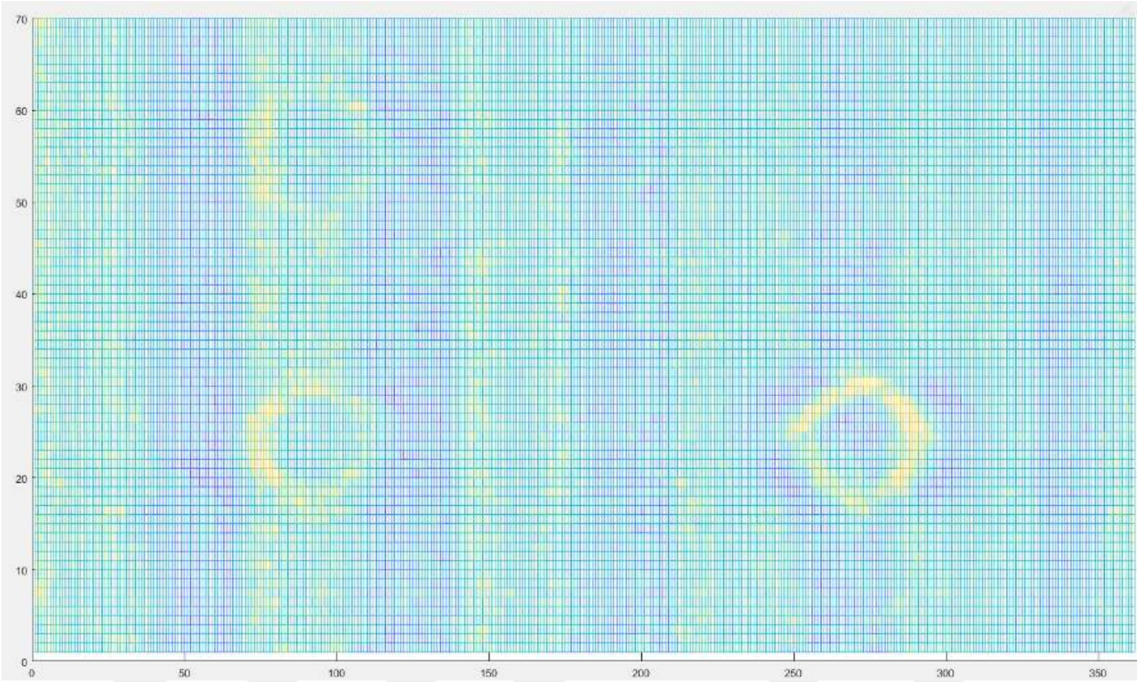

Figure 5.20 FIR filter applied to ground block eddy current data

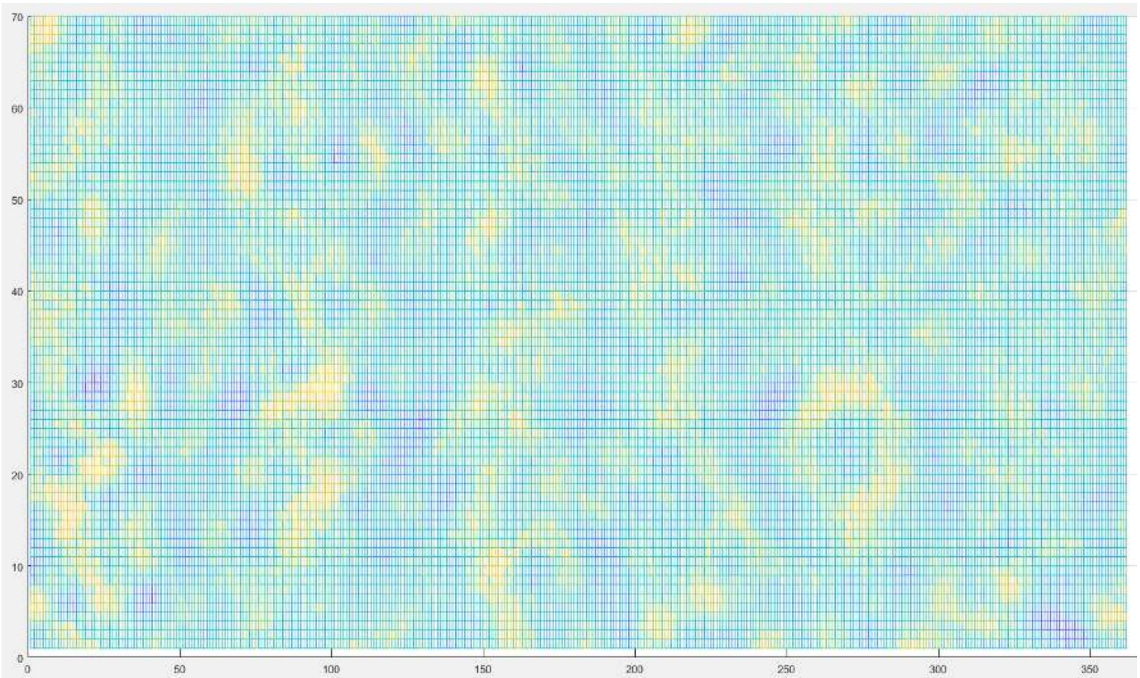

Figure 5.21 FIR filter applied to 4 defect block eddy current data

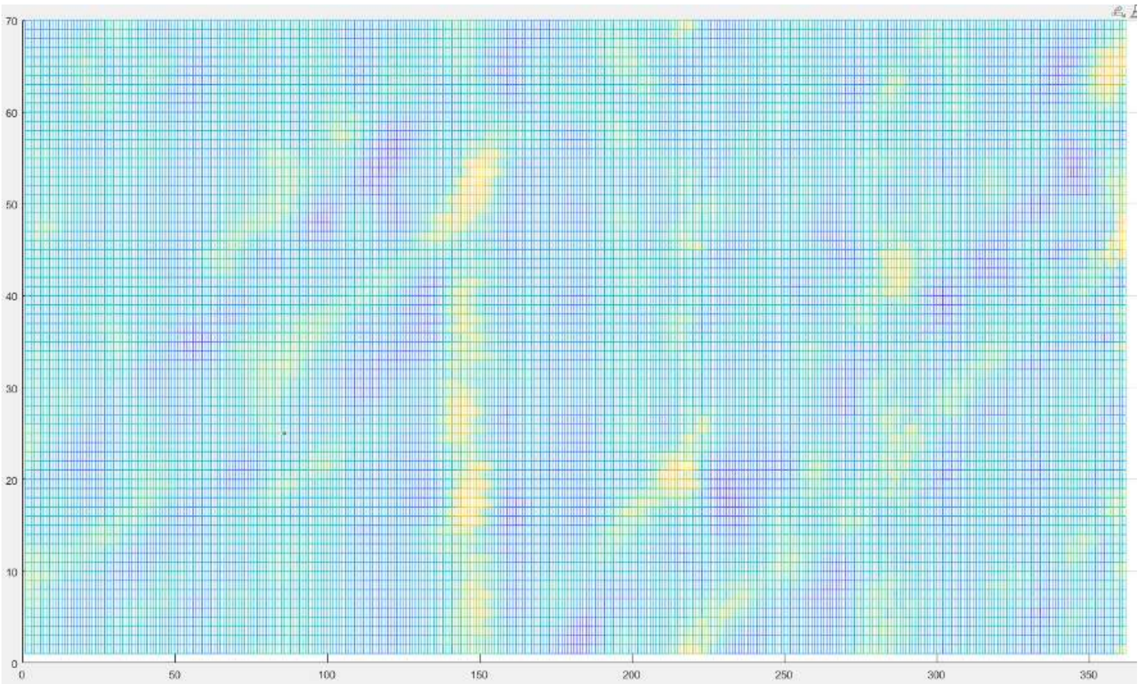

Figure 5.22 FIR filter applied to 8 defect block eddy current data

In conclusion, on the ground surface and in-process surface, 3 of the four defects are found.

- 0.750 mm length, 0.375 mm depth,
- 0.500 mm length, 0.250 mm depth,
- 1.000 mm length, 0.100 mm depth,

The shallow one of the four defects could not be identified either on ground surface or as the process surface.

- 0.200 mm length, 0.050 mm depth.

On the other hand, the shallower defects on the eight-defect block could not be separated from the total eddy current signal. This can be because possible probe vibration affected the identification analysis of shallower defects. Also, somehow surface conditions should be taken into analysis for more sensitive inspection results.

5.3 Probability of Detection

Probability of Detection (POD) is one of the essential steps of non-destructive testing. A non-destructive testing process/system must be approved for the detection ranges and confidence. The main concept of Probability of Detection is not to find how small a defect can be found but how big a defect can be missed.

In summary, an automated system, as proposed in this study, should be proved statistically for the range of detectible defect sizes. The defect size should be able to correlate to system response, and if the correlation between them is sufficient, a mathematical formula can be set between the defect size and system response for a curve fit, such as *Figure 5.23*.

When system responses on each defect have been collected, the system's capability for defect detection can be identified according to statistical measures. Such as, the example set for four different tests in Figure 5.23 gives a statistical probability detection shown in Figure 5.24.

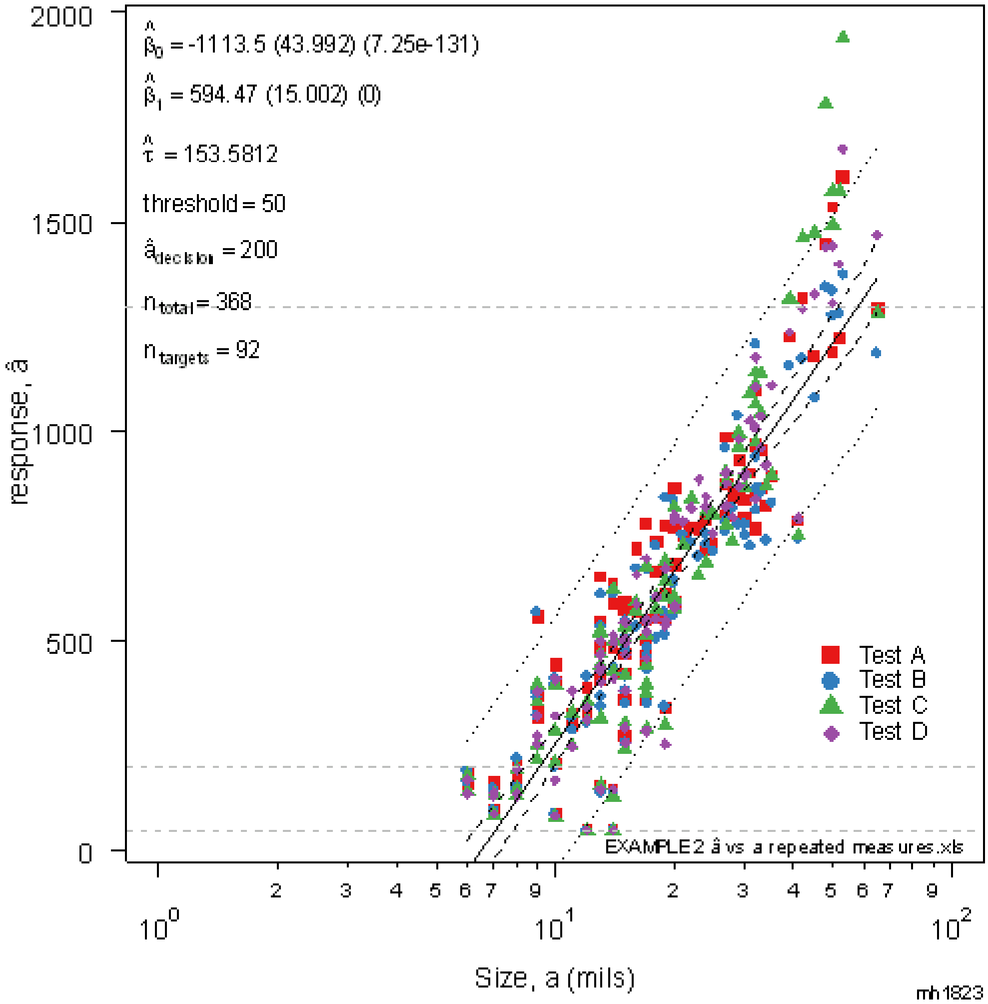

Figure 5.23 Defect size (a) vs system response (â) plot for sample data set (4 tests) [32]

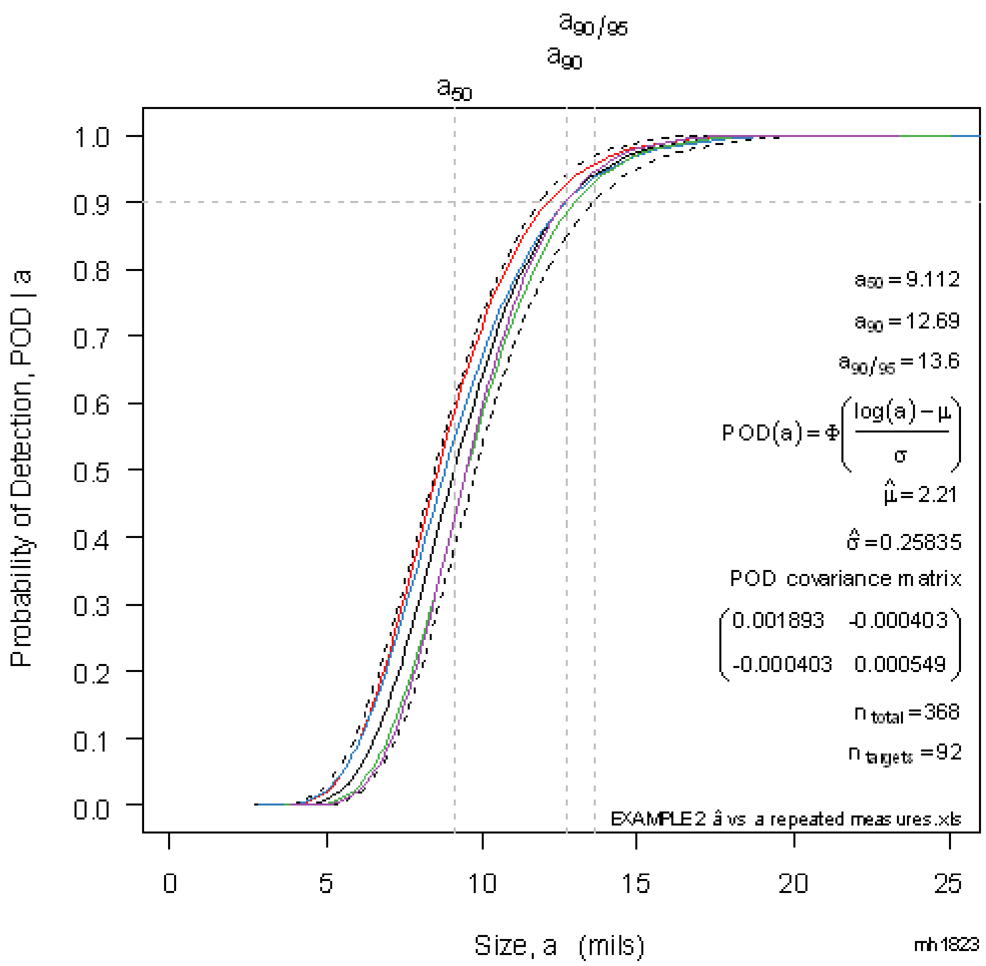

Figure 5.24 POD(a) for the data sample data set (4 test repeat) [32]

In Figure 5.24, 4 colored POD curves are shown for each test. Their statistical average POD curve is shown as a continuous black curve, and the dashed POD curves are the 95% confidence limits for the average POD curve. The general acceptability of compliance for POD analysis is a90/95, which means statistically, the threshold defect size which is giving a 90% probability of detection with 95% confidence. In Figure 5.24, this point is found as the intersections of the horizontal dashed line from 90% Probability of Detection (0.9 on the vertical axis) and positive side 95% confidence POD curve (dashed POD curved at the right side), which is 13.6 mils. For the analyzed example set it can be said that the system can find defects greater than 13.6 mils with 90% probability and 95% confidence, and the system's detection capability is not acceptable for the defects smaller than 13.6 mils.

POD is an essential task of NDT, and it will be necessary to show the confidence in the L-PBF in-process eddy current inspection.

Chapter 6

ARRAY PROBE DESIGN

6.1 Single Coil to Array Probe

Array probe is a commonly used industry demanded probe type in eddy current inspection. It has many forms and different kinds of coil orientations.

Array probes' main advantages are they can scan the surface rapidly compared to single coils, and they can be set up for changing driver and receiver coils to increase sensitivity for various kinds of defect orientations.

In this study, a single absolute coil probe is used for data collection since a snapshot of production is considered rather than making the inspection during build. But of course, in a real production environment, an array probe consisting of multiple coils should be used to decrease inspection time. Inspection time will be divided by the number of coils compared with the inspection of a single coil probe.

In this study, a single coil shielded probe with 0.750 mm coil diameter and 0.250 mm incremental spacing was found sufficient to detect defects when combined with surface laser scanning. With 0.25 mm separation of coils, the bottom view of the array probe should look as shown in Figure 6.1.

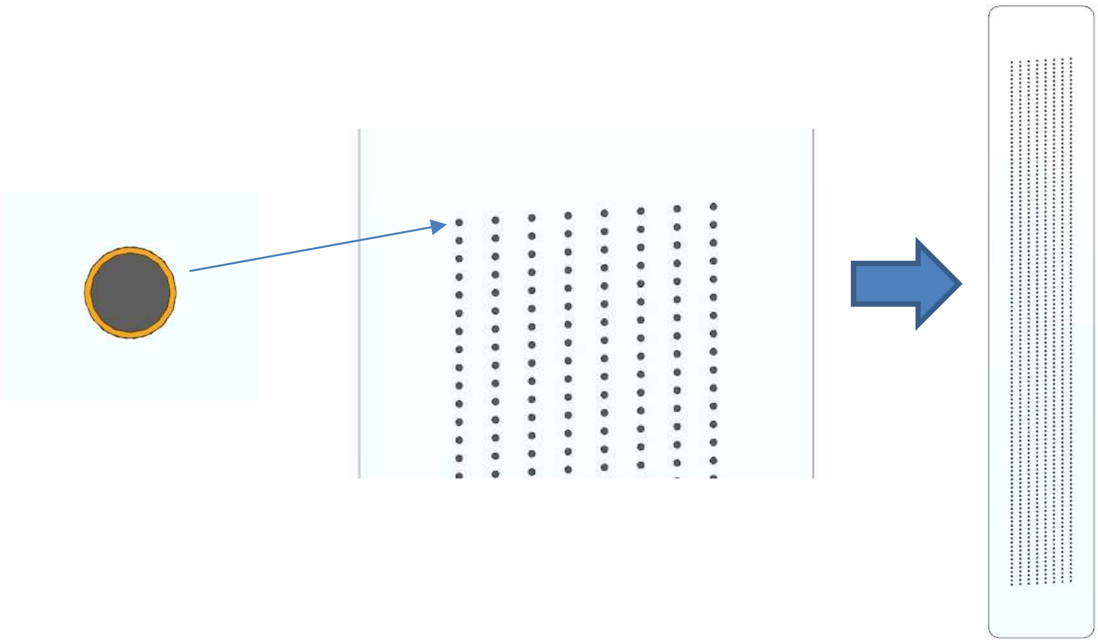

Figure 6.1 Single coil to array probe; array probe bottom view with 1000 elements in 125 rows (right)

6.1 Array Probe Design

The final array probe design can be arranged on the powder bed system shown in **Figure 6.2**, with coils looking downwards (**Figure 6.3**) to inspect the recently melted and solidified top portion of the powder bed volume.

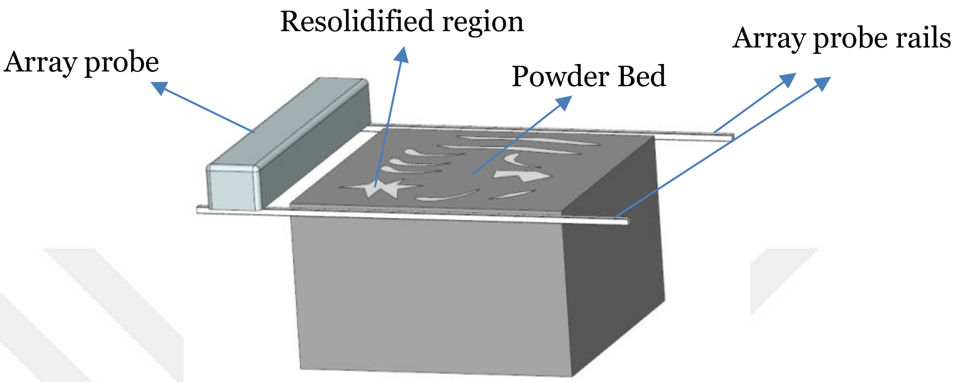

Figure 6.2 Inspection array probe arrangement on powder bed (Powder bed and array probe view only)

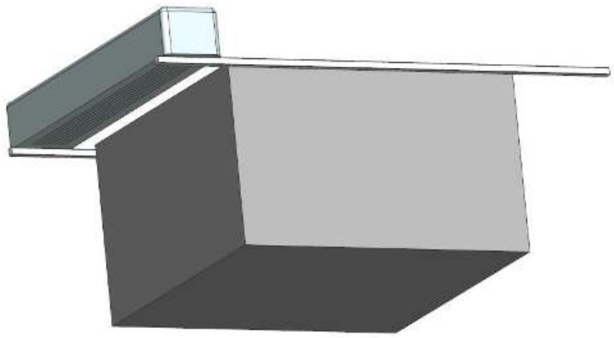

Figure 6.3 Inspection array probe, coils looking downwards

The array probe volume should include at least driver coils, receiver coils, electronic circuits, a multiplexer, and signal carrying cables or wireless communication. Soon, it will not be a surprise to see a complete bundle of the array probe volume, which also can include a small computer to run and coordinate all the circuitry, movement, data collection, laser scan point cloud data collection (if necessary) and make the analysis and send the results to the L-PBF system.

A learned best practice from this study is preventing vibration of array probe. The moving mechanism of the array probe should be as smooth as possible. Its rail system can be air cushioned or similar to anti-vibrational.

The data collection can be done as shown in Figure 6.4. The inspection probe simultaneously moves and collects data from the resolidified surface. The collected data can be used for further analysis.

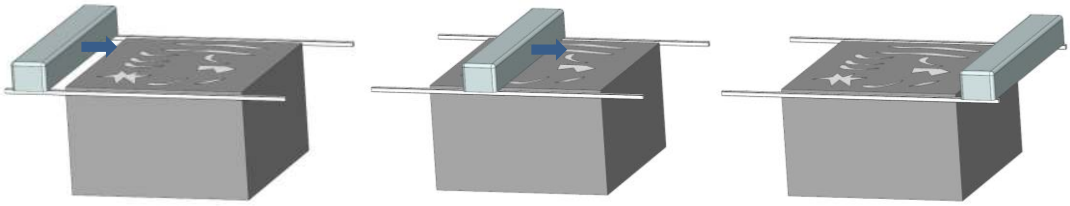

Figure 6.4 Inspection array probe surface inspection (probe moving rightwards)

Also, it can be assumed that data collection will take some tens of seconds between 2 layers' laser melting. With increasing electronics multiplexing and data rate collection technology, data collection will possibly decrease to a few seconds, like scanning a single sheet of paper on a high-speed paper copier. At that moment, the high-speed movement of the array probe (or the scanner blade) will become a problem as turbulence in the volume gas may cause disturbance of powder particles and change the flow of process gas. The turbulence can be prevented, or effects may be eliminated by using suction and gas flow outlets at the sides perpendicular to move direction.

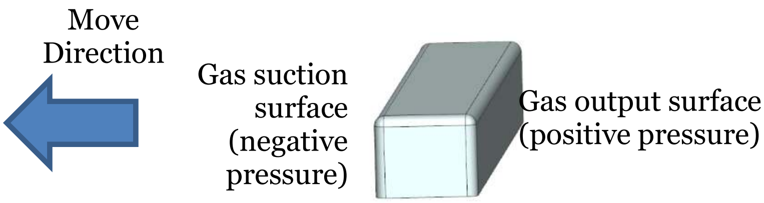

Figure 6.5 Inspection array probe view, side surface properties not to disturb powder and process gas flow (future high-speed scan)

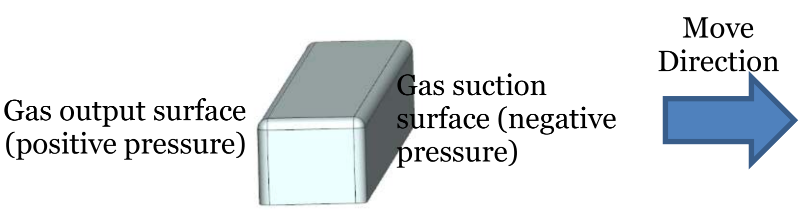

Figure 6.6 Inspection array probe view, surface characteristic changes while moving other direction (future high-speed scan)

Chapter 7

CONCLUSION & FUTURE PROSPECTS

In this study, a sample L-PBF part is produced with normal production parameters. Various kinds of defects are produced intentionally using a water-jet-guided laser system. The test part geometry is scanned using a 3D laser system. The point cloud data is used to construct the 3D image of the test part and investigate and benchmark surface conditions of the areas of inspection with eddy current data.

For eddy current inspection, a manipulator and control system have been designed and manufactured specifically for the L-PBF base plate.

Eddy current inspection data is collected using of manipulator system, and Eddyfi Ectane 2 eddy current instrument.

Python software is used to separate necessary areas from the 3D point cloud. MATLAB is used to analyze the surface eddy current data, and an FIR filter is tried for noise reduction.

In conclusion, the eddy current inspection data can detect defects during the L-PBF process. Still, care should be taken to prevent unnecessary probe vibration from increasing signal quality, and adding surface 3D surface point cloud data to analysis can improve defect detecting capability, which are the products of this thesis as novelties.

Future Study

The technology readiness level of Eddy Current inspection as L-PBF in-process monitoring is still low and assumed to reach TRL 4 in the following five years [18], a complete operating lab trial system must be manufactured, and the system capability must be proven with an “on process” Probability of Detection (POD) study. However, it is pretty unclear in the literature how to intentionally create “good” defects during the process.

FUTURE PROSPECTS

Although the major of in-process monitoring for L-PBF literature is not interested in eddy current inspection and eddy current instrument manufacturer companies have not any interest or demand for an in-process inspection array probe, eddy current inspection is seemed to be very promising for L-PBF in-process monitoring as a layer control and acceptance/certifying method. It is physically very competent as its standard depth of penetration is a few layers and covers re-solidification depth.

In recent days it may seem that eddy current inspection is widely used for industries other than additive manufacturing. Some of its best practices are based on finding defects based on eliminating inspector, surface, material, and environmental caused variables such as minor probe tilting, surface roughness, temperature difference on material, etc. The good thing about in-process L-PBF inspection is the environment is very controlled, the probe position is very known in space, and the surface condition can be measurable with the help of other techniques.

In this manner, L-PBF in-process eddy current inspection is the change of the subject inspection phenomena from a wide variety of field inspections and conventional production inspections to lab-like controlled environment in-process inspection.

It should be noted that what waited from in-process eddy-current inspection should not be on-time process parameter adjustment capability. Other methods such as infrared or visible light emitting follow-up methods should carry that load. The main objective of in-process eddy current inspection should be certifying the resolidified layer; at the end of the total build, the method should have certified each layer, and the whole build volume should be approved by this method.

The total exchangeable data rate of inspection results will possibly be practical when compared to gigabyte levels of other methods.

It should also be noted that the instrument need will require thousands of coils for large builds, which is not feasible at the state of the art when current array probes are around 256 elements maximum. This means there must be some advances necessary for probe production, such as multiplexing, data collection, and sectorial changeability of coils; for example, if a coil on the array fails, it should not scrap the whole array.

The other necessary advancements are increasing the data resolution; now, the maximum data resolution is 16 bits, and reaching higher resolutions such as 24 would give better analysis results. Also, one other advancement is the saturation of eddy current signal; if the probe on material and on-air differences exceed peak to peak voltage, then the data is saturated and may cause errors in analysis.

In conclusion, when the L-PBF process is much more advanced in process control and the build height will be totally in control, it will be the time for eddy current inspection for build certification. We can assume that in-process eddy current inspection will give layer-by-layer qualification, as it can give layer-by-layer eddy current data image. We may see this technique as a layer-by-layer inspection and imaging technique named "Eddy Current Tomography."

BIBLIOGRAPHY

[1] "5 Unstoppable Industries Using Additive Manufacturing | Stratasys Direct - Stratasys." https://www.stratasys.com/en/stratasysdirect/resources/articles/unstoppable-industries-using-additive-manufacturing/ (accessed Jul. 17, 2022).

[2] S. K. Parupelli and S. Desai, "A Comprehensive Review of Additive Manufacturing (3D Printing): Processes, Applications and Future Potential," *American Journal of Applied Sciences*, vol. 16, no. 8, 2019, doi: 10.3844/ajassp.2019.244.272.

[3] A. Gisario, M. Kazarian, F. Martina, and M. Mehrpouya, "Metal additive manufacturing in the commercial aviation industry: A review," *Journal of Manufacturing Systems*, vol. 53. 2019. doi: 10.1016/j.jmsy.2019.08.005.

[4] M. Schmidt *et al.*, "Laser based additive manufacturing in industry and academia," *CIRP Annals*, vol. 66, no. 2, 2017, doi: 10.1016/j.cirp.2017.05.011.

[5] J. A. S. , N. J. , K. H. , and S. H. Choi, "Plenary Lecture: Ultrafast laser processing to innovate consumer electronics manufacturing," Jun. 26, 2020.

[6] D. Alloys, "Digital Alloys," *https://www.digitalalloys.com/blog/application-criteria-metal-additive-manufacturing/*, Mar. 08, 2021.

[7] C. Tan, K. Zhou, W. Ma, B. Attard, P. Zhang, and T. Kuang, "Selective laser melting of high-performance pure tungsten: parameter design, densification behavior and mechanical properties," *http://www.tandfonline.com/action/journalInformation?show=aimsScope&journalCode=tsta20#.VmBmuzZFCUk*, vol. 19, no. 1, pp. 370–380, Dec. 2018, doi: 10.1080/14686996.2018.1455154.

[8] M. E. Arbabian and M. R. Wagner, "The impact of 3D printing on manufacturer–retailer supply chains," *European Journal of Operational Research*, vol. 285, no. 2, 2020, doi: 10.1016/j.ejor.2020.01.063.

[9] R. Stolt, F. Elgh, and T. Heikkinen, "Design and evaluation of aerospace components for SLM," in *Advances in Transdisciplinary Engineering*, 2019, vol. 10. doi: 10.3233/ATDE190119.

[10] E. Kundakcioglu, I. Lazoglu, and S. Rawal, "Transient thermal modeling of laser-based additive manufacturing for 3D freeform structures," *International Journal of Advanced Manufacturing Technology*, vol. 85, no. 1–4, 2016, doi: 10.1007/s00170-015-7932-2.

[11] E. Kundakcıoğlu, I. Lazoglu, Ö. Poyraz, E. Yasa, and N. Cizicioğlu, "Thermal and molten pool model in selective laser melting process of Inconel 625," *International Journal of Advanced Manufacturing Technology*, vol. 95, no. 9–12, 2018, doi: 10.1007/s00170-017-1489-1.

[12] N. Tepylo, X. Huang, and P. C. Patnaik, "Laser-Based Additive Manufacturing Technologies for Aerospace Applications," *Advanced Engineering Materials*, vol. 21, no. 11. 2019. doi: 10.1002/adem.201900617.

[13] N. Ortega, S. Martínez, I. Cerrillo, A. Lamikiz, and E. Ukar, "Computed tomography approach to quality control of the Inconel 718 components obtained by additive manufacturing (SLM)," *Procedia Manufacturing*, vol. 13, pp. 116–123, 2017, doi: 10.1016/j.promfg.2017.09.018.

[14] C. Laser, "Concept Laser Process Monitoring," *https://www.ge.com/additive/sites/default/files/2018-02/1708_QM-pm_EN_update_1__lowres_einzel.pdf*, May 22, 2021.

[15] EOS, "EOSTATE Melt Pool," *https://www.eos.info/en/additive-manufacturing/software-3d-printing/monitoring-software#meltpool*, May 22, 2021.

[16] EOS, "EOS EOSTATE Exposure OT video," *https://www.eos.info/en/additive-*

manufacturing/software-3d-printing/monitoring-software#video_19814, May 22, 2021.
[17] "Progress Report on AMSC Roadmap v2 Gaps-April 2022 Progress Report on AMSC Roadmap v2 Gaps," 2022.
[18] E. Lanigan, "In-Situ Technology Readiness for Applications in AM Qualification and Certification Workshop," Jun. 22, 2022.
[19] M. Abdelrahman, E. W. Reutzel, A. R. Nassar, and T. L. Starr, "Flaw detection in powder bed fusion using optical imaging," *Additive Manufacturing*, vol. 15, 2017, doi: 10.1016/j.addma.2017.02.001.
[20] M. Montazeri, A. R. Nassar, A. J. Dunbar, and P. Rao, "In-process monitoring of porosity in additive manufacturing using optical emission spectroscopy," *IISE Transactions*, 2020, doi: 10.1080/24725854.2019.1659525.
[21] G. Mohr *et al.*, "In-situ defect detection in laser powder bed fusion by using thermography and optical tomography—comparison to computed tomography," *Metals (Basel)*, vol. 10, no. 1, 2020, doi: 10.3390/met10010103.
[22] W. He, W. Shi, J. Li, and H. Xie, "In-situ monitoring and deformation characterization by optical techniques; part I: Laser-aided direct metal deposition for additive manufacturing," *Optics and Lasers in Engineering*. 2019. doi: 10.1016/j.optlaseng.2019.05.020.
[23] M. Khanzadeh, W. Tian, A. Yadollahi, H. R. Doude, M. A. Tschopp, and L. Bian, "Dual process monitoring of metal-based additive manufacturing using tensor decomposition of thermal image streams," *Additive Manufacturing*, 2018, doi: 10.1016/j.addma.2018.08.014.
[24] S. P. Santospirito, K. Słyk, B. Luo, R. Łopatka, O. Gilmour, and J. Rudlin, "Detection of defects in laser powder deposition (LPD) components by pulsed laser transient thermography," in *Thermosense: Thermal Infrared Applications XXXV*, 2013, vol. 8705. doi: 10.1117/12.2016139.
[25] B. M. Colosimo and M. Grasso, "In-situ monitoring in L-PBF: Opportunities and challenges," 2020. doi: 10.1016/j.procir.2020.09.151.
[26] E. I. Todorov, "Eddy Current Technologies for Real-Time Monitoring and Post-Process Examination of Laser Powder Bed Fusion Process," in *Structural Integrity of Additive Manufactured Parts*, ASTM International, 2020, pp. 129–164. doi: 10.1520/stp162020180132.
[27] E. I. Todorov, "Nondestructive Testing and Evaluation," in *Encyclopedia of Materials: Metals and Allloys*, Elsevier, 2022, pp. 168–192. doi: 10.1016/b978-0-12-819726-4.00145-9.
[28] NDT Resource Center, "NDT Resource Center," *https://www.nde-ed.org/EducationResources/CommunityCollege/EddyCurrents/Physics/PopUps/picpopup3.htm*, Feb. 07, 2021.
[29] "Nondestructive Evaluation Physics : Electricity." https://www.nde-ed.org/Physics/Electricity/depthcurrentdensity.xhtml (accessed Jul. 11, 2022).
[30] "Nondestructive Evaluation Techniques : Eddy Current Testing." https://www.nde-ed.org/NDETechniques/EddyCurrent/Instrumentation/impedanceplane.xhtml (accessed Jul. 11, 2022).
[31] Synova, "Synova Laser Microjet," *https://www.synova.ch/technology/laser-microjet.html*, Jun. 12, 2022.
[32] U. DoD, "MIL-HDBK-1823A Nondestructive Evaluation System Reliability Assessment," 2009.

Appendix A

List and mapping of defects

Nm : Notch middle (location from mid-point)
Ne : Notch edge (location from edge point)
H : Hole
X : Defect X-axis coordinate (mm)
Y : Defect Y-axis coordinate (mm)
L : Length of defect (mm)
Θ : Angle of notch (degree)
Φ : Diameter of hole (mm)
D : Depth of defect (mm)

Defect #	Defect Type	X	Y	L	θ	ϕ	D
1	Nm	10	7	0.75	90		0.375
2	Nm	20	7	0.5	90		0.25
3	Nm	10	14	0.2	90		0.04
4	Nm	20	14	1	90		0.1
5	Nm	70	7	0.75	90		0.375
6	Nm	80	7	0.5	90		0.25
7	Nm	70	14	0.2	90		0.08
8	Nm	80	14	1	90		0.1
9	Nm	-54	7	1	90		0.12
10	H	-48	7			0.4	0.2
11	Nm	-42	7	1	90		0.2
12	H	-36	7			0.3	0.2
13	H	-54	14			0.2	0.2
14	Nm	-48	14	1	90		0.08
15	H	-42	14			0.1	0.2
16	Nm	-36	14	1	90		0.04
17	Nm	-28	41	1.5	45		0.12
18	Nm	-36	41	1	45		0.16
19	H	-28	49			0.3	0.12
20	H	-36	49			0.15	0.16
21	Ne	-22	55	0.75	225		0.12
22	Ne	-22	35	0.75	135		0.04
23	Ne	-53	35	2	90		0.12
24	Ne	-59	35	2	45		0.08
25	Ne	-66	35	1	135		0.16
26	Nm	-53	45	0.75	90		0.04
27	Nm	-59	45	0.75	90		0.16
28	Ne	-66	45	1	180		0.12

29	Ne	-53	55	1	270		0.16
30	Ne	-59	55	2.4	270		0.16
31	Ne	-66	55	1	225		0.16
32	Ne	-28	60	2	90		0.12
33	Ne	-34	60	2	45		0.08
34	Ne	-40.5	60	1.5	135		0.16
35	Nm	-28	70	0.75	90		0.04
36	Nm	-34	70	0.75	90		0.16
37	Ne	-40.5	70	1.5	180		0.12
38	Ne	-28	80	1	270		0.16
39	Ne	-34	80	2.4	270		0.16
40	Ne	-40.5	80	1.5	225		0.16
41	Ne	-53	60	2	90		0.12
42	Ne	-59	60	2	45		0.08
43	Ne	-65	60	2	135		0.16
44	Nm	-53	70	0.75	90		0.04
45	Nm	-59	70	0.75	90		0.16
46	Ne	-65	70	2	180		0.12
47	Ne	-28	85	2	90		0.12
48	Ne	-34	85	2	45		0.08
49	Ne	-39.5	85	2.5	135		0.16
50	Nm	-28	95	0.75	90		0.04
51	Nm	-34	95	0.75	90		0.16
52	Ne	-39.5	95	2.5	180		0.12
53	Ne	-53	85	2	90		0.12
54	Ne	-59	85	2	45		0.08
55	Ne	-64	85	3	135		0.16
56	Nm	-53	95	0.75	90		0.04
57	Nm	-59	95	0.75	90		0.16
58	Ne	-64	95	3	180		0.12
59	Nm	32	41	1.5	45		0.12
60	Nm	24	41	1	45		0.16
61	H	32	49			0.3	0.12
62	H	24	49			0.15	0.16
63	Ne	38	55	0.75	225		0.12
64	Ne	38	35	0.75	135		0.04
65	Ne	7	35	2	90		0.12
66	Ne	1	35	2	45		0.08
67	Ne	-6	35	1	135		0.16
68	Nm	7	45	0.75	90		0.04
69	Nm	1	45	0.75	90		0.16
70	Ne	-6	45	1	180		0.12
71	Ne	7	55	1	270		0.16
72	Ne	1	55	2.4	270		0.16
73	Ne	-6	55	1	225		0.16

74	Ne	32	60	2	90		0.12
75	Ne	26	60	2	45		0.08
76	Ne	19.5	60	1.5	135		0.16
77	Nm	32	70	0.75	90		0.04
78	Nm	26	70	0.75	90		0.16
79	Ne	19.5	70	1.5	180		0.12
80	Ne	32	80	1	270		0.16
81	Ne	26	80	2.4	270		0.16
82	Ne	19.5	80	1.5	225		0.16
83	Ne	7	60	2	90		0.12
84	Ne	1	60	2	45		0.08
85	Ne	-5	60	2	135		0.16
86	Nm	7	70	0.75	90		0.04
87	Nm	1	70	0.75	90		0.16
88	Ne	-5	70	2	180		0.12
89	Ne	32	85	2	90		0.12
90	Ne	26	85	2	45		0.08
91	Ne	20.5	85	2.5	135		0.16
92	Nm	32	95	0.75	90		0.04
93	Nm	26	95	0.75	90		0.16
94	Ne	20.5	95	2.5	180		0.12
95	Ne	7	85	2	90		0.12
96	Ne	1	85	2	45		0.08
97	Ne	-4	85	3	135		0.16
98	Nm	7	95	0.75	90		0.04
99	Nm	1	95	0.75	90		0.16
100	Ne	-4	95	3	180		0.12
101	Nm	92	41	1.5	45		0.04
102	Nm	84	41	0.4	45		0.12
103	H	92	49			0.3	0.12
104	H	84	49			0.15	0.16
105	Ne	98	55	0.25	225		0.12
106	Ne	98	35	0.25	135		0.04
107	Ne	67	35	3	90		0.12
108	Ne	61	35	3	45		0.16
109	Ne	92	60	3	90		0.12
110	Ne	84	60	3	45		0.16
111	Ne	67	60	3	90		0.12
112	Ne	61	60	3	45		0.16
113	Ne	92	85	3	90		0.12
114	Ne	84	85	3	45		0.16
115	Ne	67	85	3	90		0.12
116	Ne	61	85	3	45		0.16
117	Nm	-47	125	8	90		0.12
118	Ne	-21	121	1.5	270		0.08

119	Ne	-17	124	1	0		0.04
120	Ne	-25	124	0.75	180		0.16
121	Ne	-21	127	0.75	90		0.08
122	Ne	4	117	1.5			0.12
123	Ne	12	124	1			0.08
124	Nm	4	124	0.25	90		0.04
125	Ne	-4	124	0.75			0.04
126	Ne	4	131	0.75			0.16
127	Nm	54	124	0.25	45		0.04
128	H	79	124			0.1	0.04
129	Nm	-53	139	0.35	45		0.08
130	H	-39	139			0.2	0.08
131	Nm	-22	139	0.65	90		0.12
132	H	-9	139			0.15	0.04
133	Ne	4	140	0.65	270		0.12
134	Ne	21	140	0.65	270		0.08
135	H	57	140			0.15	0.08
136	Nm	-50	109	1	45		0.04
137	Nm	-30	109	1	45		0.12
138	Ne	-15	108	1.5	45		0.08
139	Ne	-1	108	1.5	90		0.04
140	Ne	15.7	108	0.5	90		0.08
141	Ne	39	108	0.5	45		0.12
142	Nm	-45.4	215.5	1.5	45		0.16
143	H	-31.6	217.7			0.3	0.16
144	Nm	-40.9	207.5	0.75	45		0.16
145	Nm	-30.1	208.3	0.75	45		0.2
146	Nm	-34.5	199.3	0.75	45		0.24
147	Ne	-20.9	195.3	0.75	0		0.2
148	Ne	-18.4	184.8	0.75	180		0.28
149	Ne	-12.7	199.8	0.75	0		0.24
150	Ne	-9.5	187	0.75	90		0.2
151	Ne	-0.8	199.8	0.75	180		0.16
152	Ne	-1.8	182.7	0.75	0		0.12
153	Ne	-5	171.6	0.75	180		0.08
154	Nm	19.5	194.5	1	90		0.12
155	Nm	30.8	201.5	0.25	90		0.12
156	Nm	42.6	211.8	1	90		0.2
157	Nm	62	219.8	0.25	90		0.2
158	Nm	27.4	181.5	1	90		0.08
159	Nm	36.3	184.2	0.25	90		0.08
160	Nm	49	205.1	1	90		0.04
161	Nm	62	209.6	0.25	90		0.04
162	Nm	24.4	163.7	0.15	90		0.04
163	Nm	45.3	184.5	0.15	90		0.2

164	H	68.3	190.9			0.75	0.2
165	H	83.9	202.6			1	0.2
166	H	41.7	160.9			1	0.04
167	H	52	166			0.75	0.04
168	H	75.3	179.3			0.25	0.2
169	H	87.6	187.3			0.25	0.04
170	H	52	148.7			0.2	0.12
171	H	68.3	151.7			0.1	0.08
172	H	91	168.7			0.15	0.04
173	Ne	-16.4	205.7	0.4	45		0.12
174	Ne	-10.8	213.2	0.6	0		0.12
175	Ne	-15.4	174.1	0.48	0		0.16
176	H	-20.4	175.3			0.24	0.2
177	H	-40.4	174.8	0.75	45	0.22	0.12
178	Ne	-32.8	170.1	0.54	0		0.16
179	Nm	-16	167.4	0.68	30		0.28
180	H	-27.9	163.7			0.95	0.16
181	Ne	-42.4	164.5	0.45	120		0.2
182	Nm	-8.7	161.6	0.37	45		0.16
183	Ne	-36.7	152.2	0.55	160		0.2
184	H	-33.1	227.4			0.43	0.08
185	H	-25.9	226.4			0.65	0.12
186	H	-11.1	221.8			0.55	0.16
187	H	-0.7	213			0.35	0.04
188	H	6.4	199.5			0.7	0.08

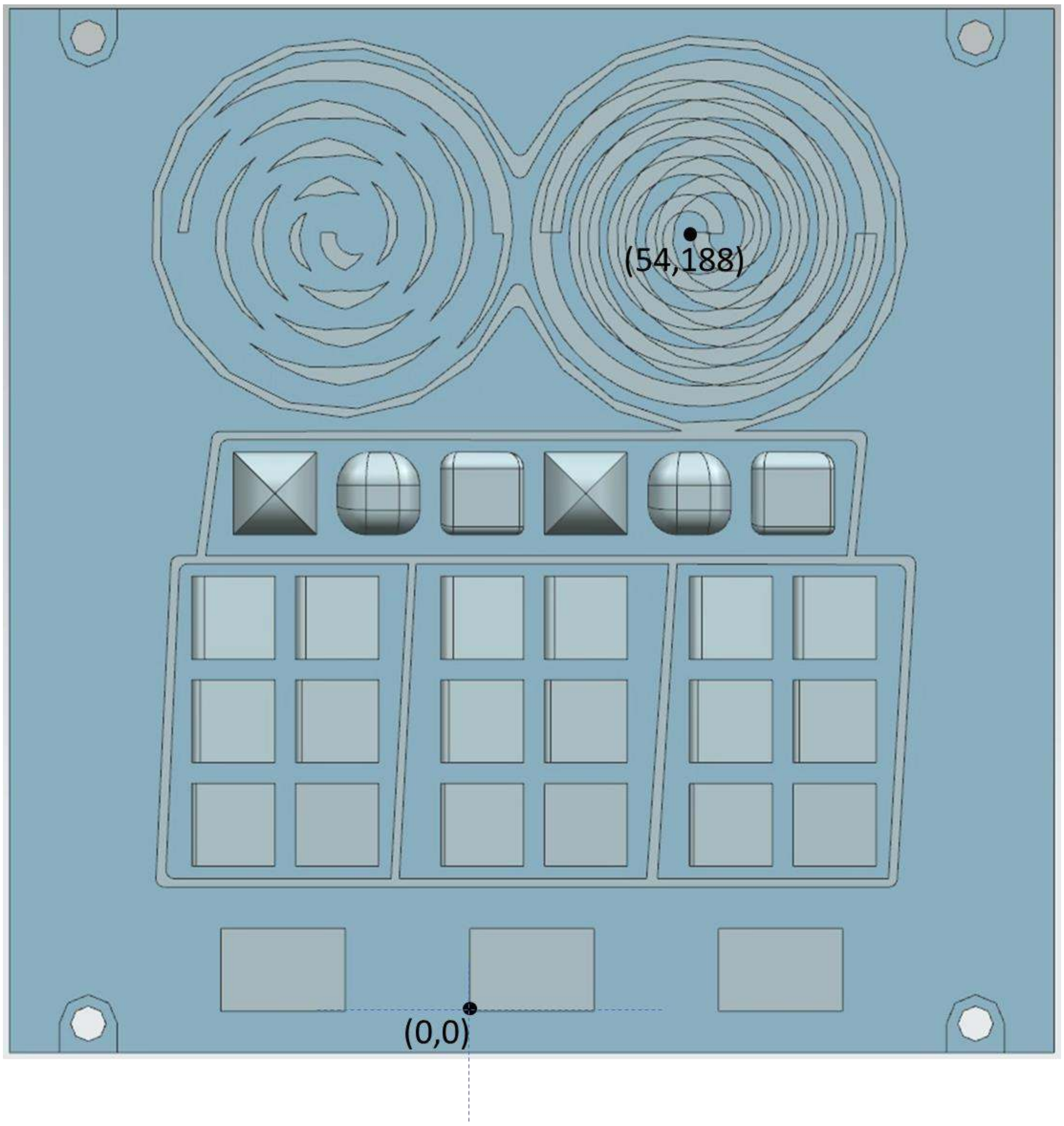
(54,188)
(0,0)

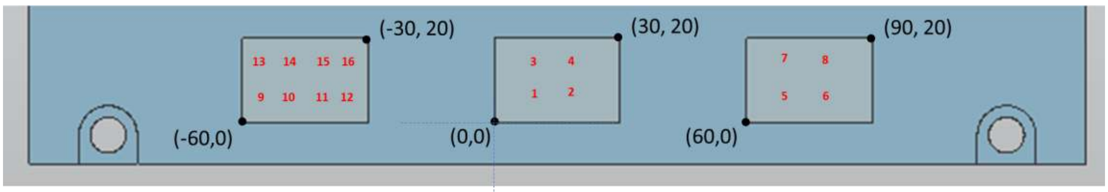
(-30, 20)
(30, 20)
(90, 20)
13 14 15 16
9 10 11 12
3 4
1 2
7 8
5 6
(-60,0)
(0,0)
(60,0)

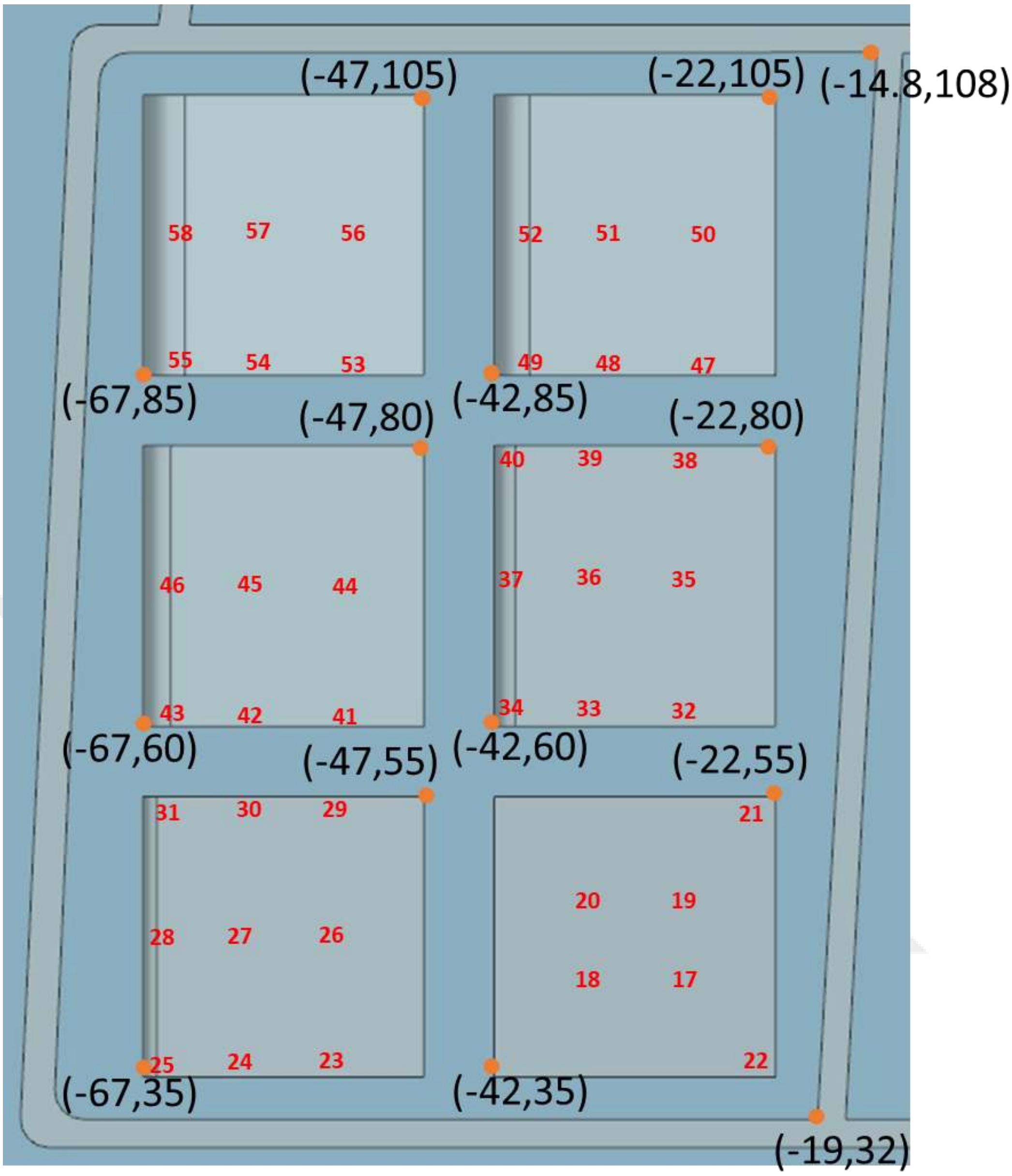
(-47,105)
(-22,105)
(-14.8,108)
58
57
56
52
51
50
55
54
53
49
48
47
(-67,85)
(-47,80)
(-42,85)
(-22,80)
40
39
38
46
45
44
37
36
35
43
42
41
34
33
32
(-67,60)
(-47,55)
(-42,60)
(-22,55)
31
30
29
21
20
19
28
27
26
18
17
25
24
23
22
(-67,35)
(-42,35)
(-19,32)

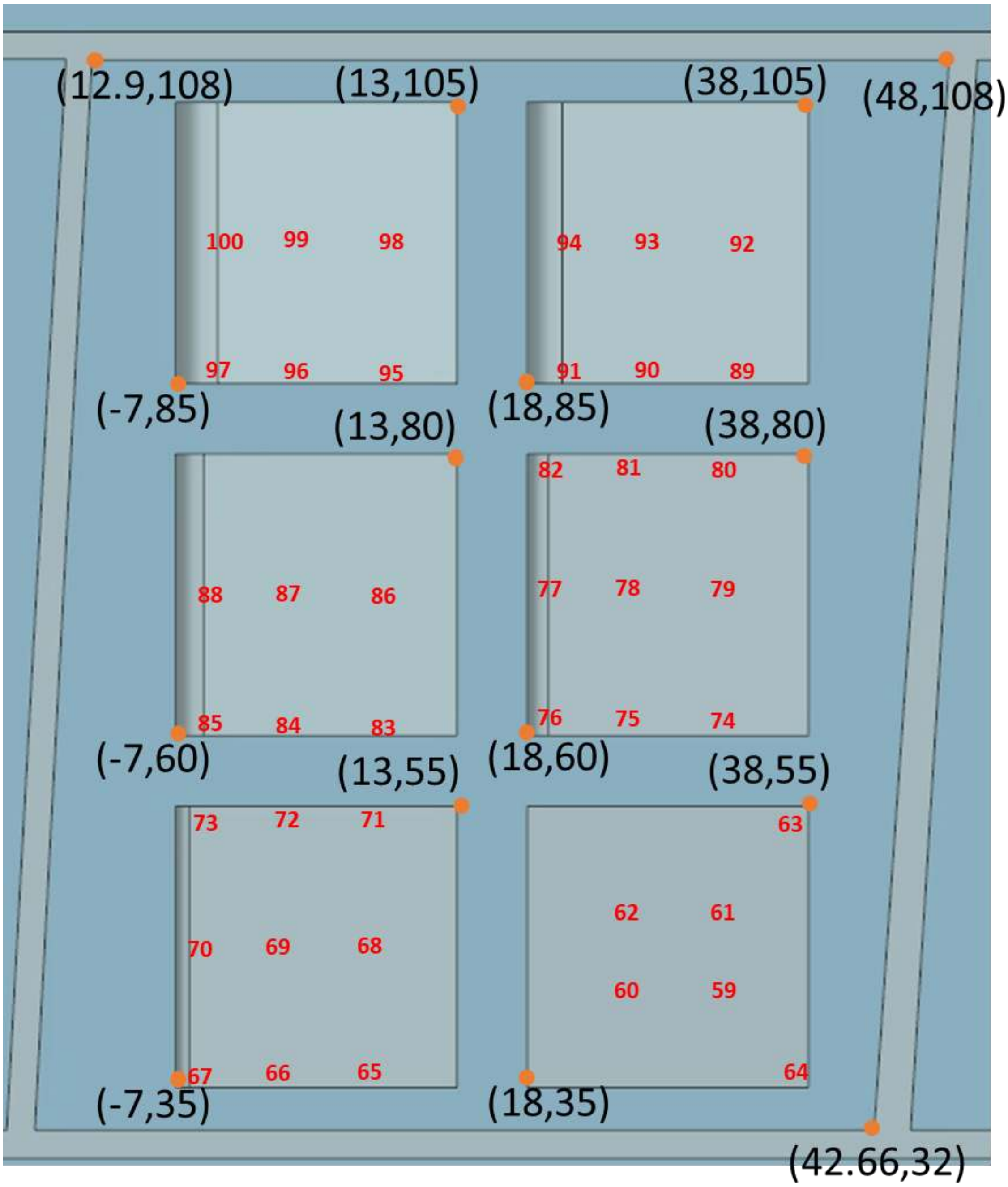
(12.9,108)
(13,105)
(38,105)
(48,108)
100
99
98
94
93
92
97
96
95
91
90
89
(-7,85)
(13,80)
(18,85)
(38,80)
82
81
80
88
87
86
77
78
79
85
84
83
76
75
74
(-7,60)
(13,55)
(18,60)
(38,55)
73
72
71
63
62
61
70
69
68
60
59
67
66
65
64
(-7,35)
(18,35)
(42.66,32)

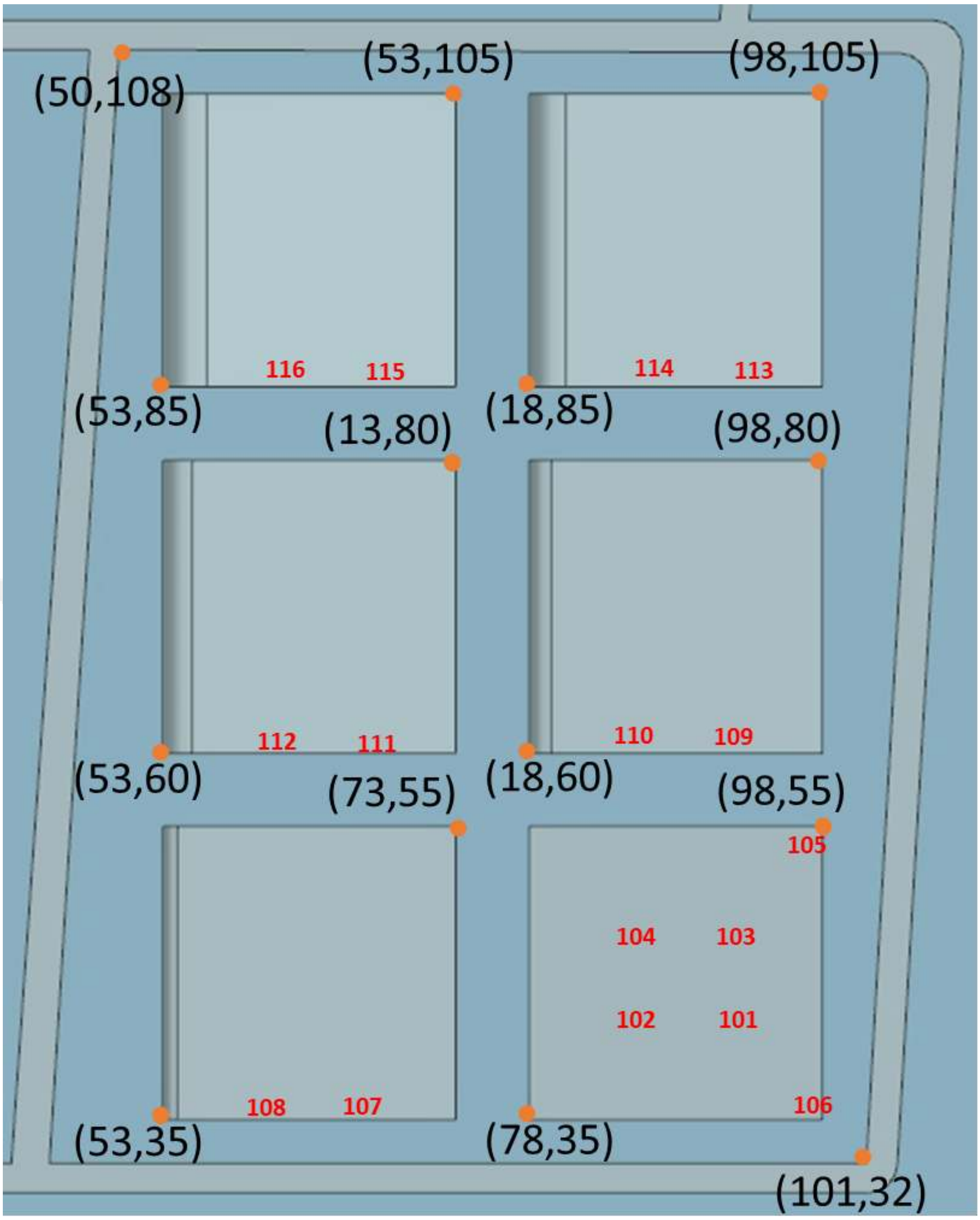
(50,108)
(53,105)
(98,105)
116
115
114
113
(53,85)
(13,80)
(18,85)
(98,80)
112
111
110
109
(53,60)
(73,55)
(18,60)
(98,55)
105
104
103
102
101
108
107
106
(53,35)
(78,35)
(101,32)

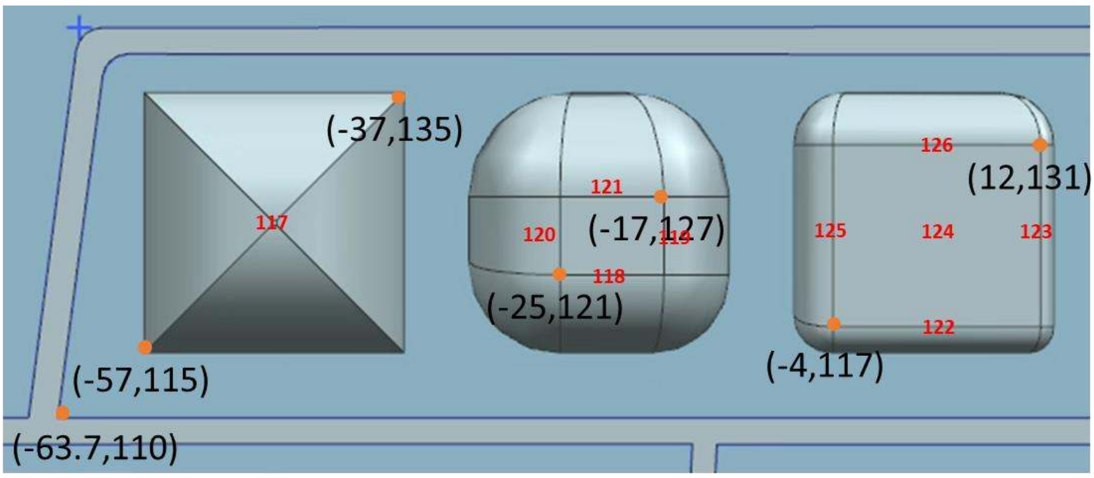
(-37,135)
117
121
120
(-17,127)
119
118
(-25,121)
126
(12,131)
125
124
123
122
(-57,115)
(-4,117)
(-63.7,110)

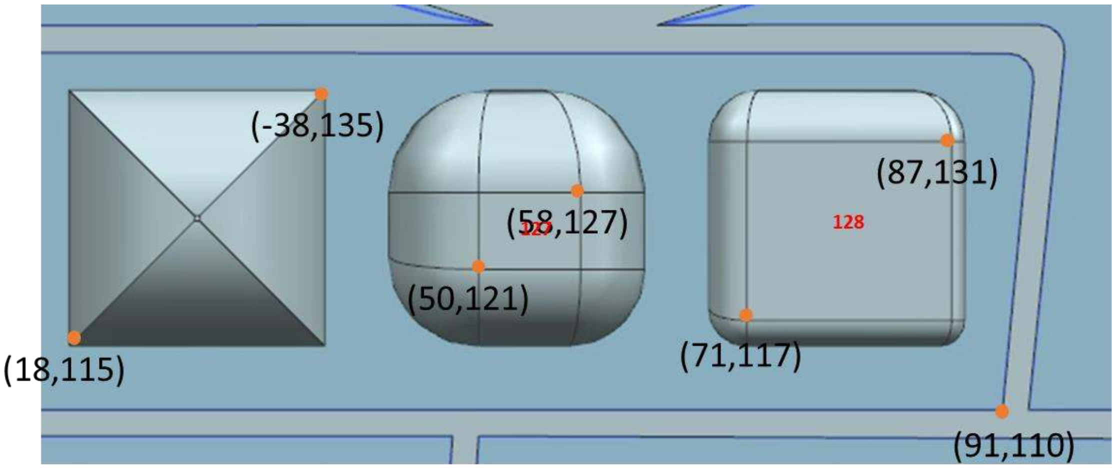
(-38,135)
(58,127)
(50,121)
(18,115)
128
(87,131)
(71,117)
(91,110)

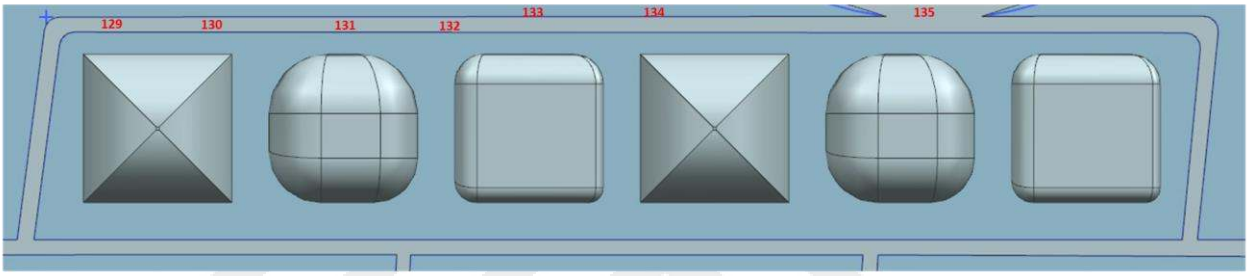
129
130
131
132
133
134
135

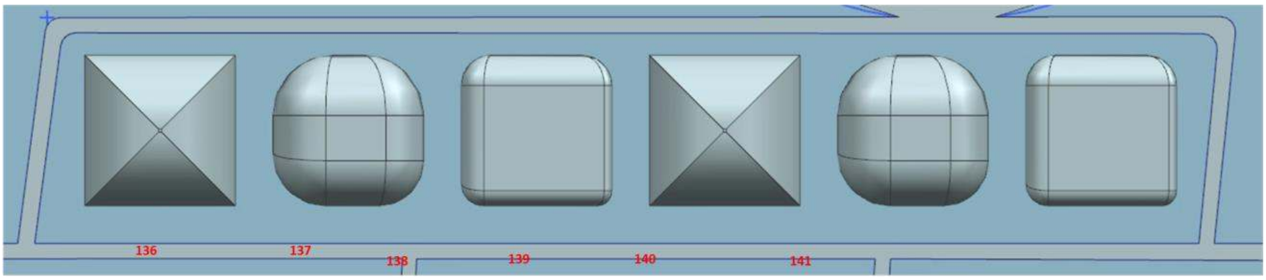
136
137
138
139
140
141

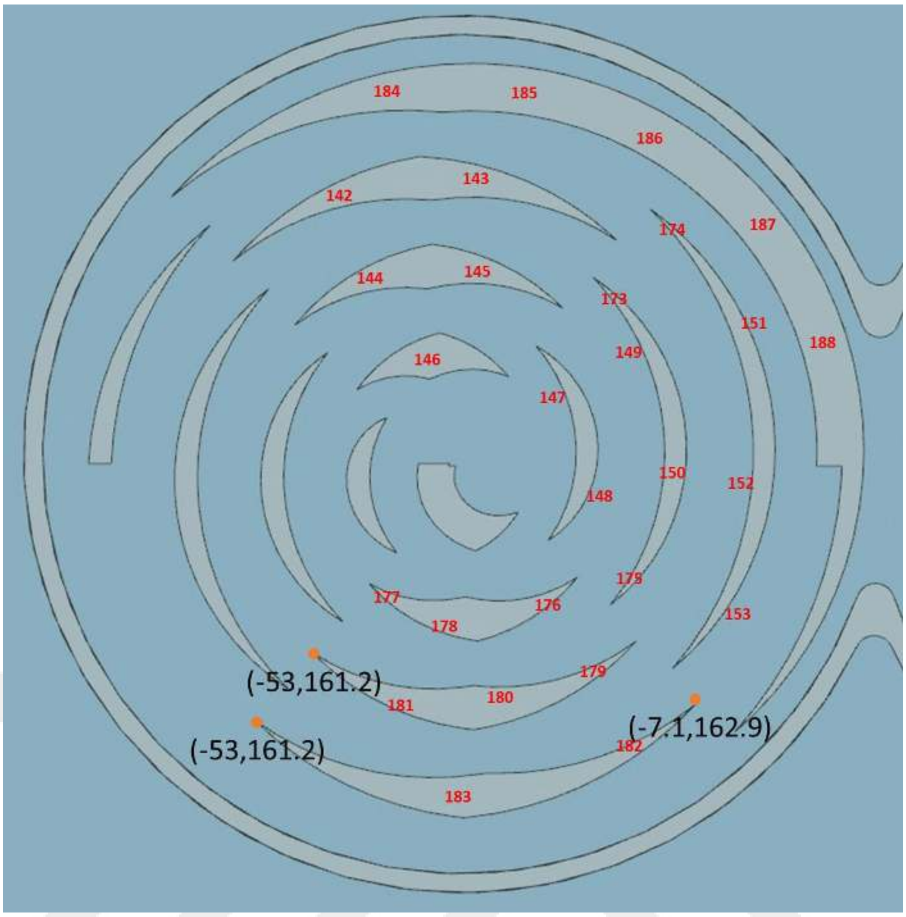
184
185
186
142
143
174
187
144
145
173
151
188
146
149
147
150
152
148
175
177
176
153
178
(-53,161.2)
179
181
180
(-53,161.2)
182
(-7.1,162.9)
183

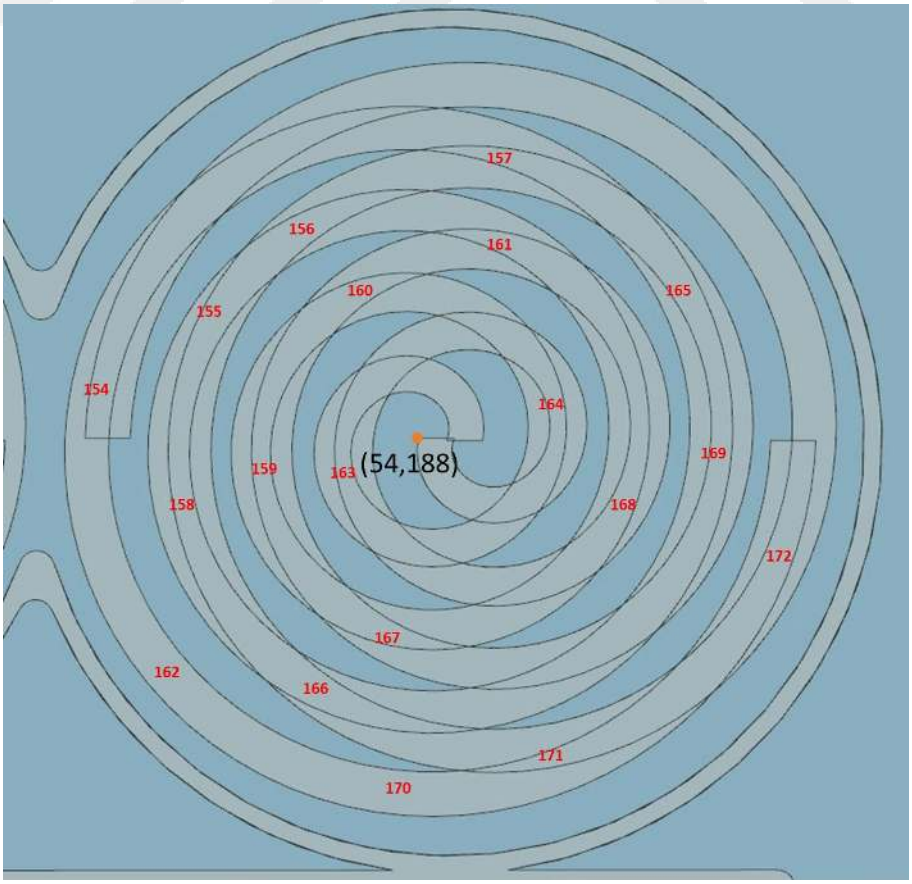
157
156
161
160
165
155
154
164
(54,188)
169
159
163
158
168
172
167
162
166
171
170